Thermodynamic modelling of composition and crystal structure of ternary nanowires

Leshchenko, Egor

2020

LICENTIATE THESIS

THERMODYNAMIC MODELLING OF COMPOSITION AND CRYSTAL STRUCTURE OF TERNARY NANOWIRES

Author:

EGOR LESHCHENKO

Main supervisor:

Assoc. Prof. Jonas Johansson

Co-supervisor:

Assoc. Prof. Martin H. Magnusson

Division of Solid State Physics

Department of Physics

Lund University

2020

Division of Solid State Physics
Department of Physics
Lund University
Box 118
S-22100 Lund
Sweden

Contents

Abstract

III-V semiconductor nanowires exhibit truly unique properties different from their bulk counterparts and they have several promising applications in optoelectronics, biotechnology and energy harvesting. A critical step in the NW-based device design is the ability to control the composition and crystal structure of ternary III-V nanowires. Such tuning is impossible without understanding of the underlying growth mechanism. Theoretical modelling may provide insight into the growth processes and help to assess optimal growth conditions. In this perspective, an analytical approach for fundamental understanding of ternary nanowire formation has been developed. This approach concerns two aspects, namely the composition and crystal phase control.

Within the first aspect, we consider the formation of a ternary nucleus from a quaternary liquid and calculate the chemical potential difference which is the driving force for nanowire growth. In so doing, we have derived an analytic expression for the composition of a ternary solid material nucleating from a quaternary liquid melt. It is based on two-component nucleation theory with realistic thermodynamic descriptions of the liquid and solid phases. We have applied this theory to Au-catalyzed and self-catalyzed, nucleation limited vapor-liquid-solid growth of ternary III-V nanowires. We discuss in details the composition of nanowires of In-Ga-As-Au, Al-Ga-As-Au, In-Ga-Sb-Au and In-Sb-As-Au materials systems.

Next, within the second aspect, we apply the developed model for the description of the formation of a ternary nucleus which can exhibit the zinc blende or wurtzite structures. In order to do so, we introduce the difference in the cohesive energy between the zinc blende and wurtzite structures. Then we calculate the size of the critical nuclei and the nucleation rates by minimizing the formation energy. As a result, we get a model for the composition dependence of the zinc blende – wurtzite polytypism in ternary nanowires growing by the vapor-liquid-solid mechanism.

List of Papers

This licentiate thesis is based on the following two articles:

I. Nucleation-limited composition of ternary III-V nanowires forming from quaternary gold based liquid alloys
Egor D. Leshchenko, Masoomeh Ghasemi, Vladimir G. Dubrovskii, Jonas Johansson. *CrystEngComm*, 2018, **20**, 1649 – 1655.

II. Zinc blende and wurtzite crystal structure formation in gold catalyzed InGaAs nanowires
Jonas Johansson, **Egor D. Leshchenko**, *Journal of Crystal Growth*, 2019, **509**, 118-123.

The following article is not included in the thesis, however it is related to the composition control of ternary nanowires:

III. Nucleation limited composition of $Al_{1-x}In_xAs$ nanowires
Egor D. Leshchenko, Vladimir G. Dubrovskii, Jonas Johansson, *J. Phys.: Conf. Ser.*, 2019, 1199, 012022

List of Abbreviations and Notations

$E_{\mathrm{g,AD}}$	band gaps
ΔA	change of drop surface
μ_i	chemical potential of the species i
S^m	configurational entropy
H	enthalpy
S	entropy
R	gas constant
G	Gibbs free energy
G_i^0	Gibbs free energy of pure elements
G^{ex}	(binary, ternary or high order) excess Gibbs energy
F	Helmholtz free energy
ω_{ij}	binary interaction parameter
ω_{ijk}	ternary interaction parameter
ω_s	pseudo-binary interaction parameter
U	internal energy
a_{AD}	lattice parameter
h	layer height
γ_{LV}	liquid-vapor surface energy
x_i	mole fraction of component i
s	number of III-V pairs in the nucleus
N	number of components
n_i	particle number of species i
P_n	perimeter
P	pressure
ζ	supersaturation
T	temperature
V	volume
HVPE	hydride vapor-phase epitaxy
MBE	molecular beam epitaxy
MOVPE	metal organic vapor phase epitaxy
NW	nanowire
VLS	vapor-liquid-solid (mechanism)

Acknowledgments

First and foremost, I would like to say thank you to my supervisor, Jonas Johansson. Thank you for giving me support and encouragement. You inspire me to move forward and to develop new ideas.

I thank my co-supervisor Martin Magnusson for the help and nice discussions.

I am incredibly grateful to Vladimir Dubrovskii my previous supervisor. You taught me how to work hard and achieve the goal.

Thanks to my co-worker Masoomeh Ghasemi for the help in CALPHAD learning and collaboration.

An extra thank you to my lecturers who taught me and to all the friendly people at Solid State Physics.

Egor Leshchenko
Lund University
27 January 2020

Chapter 1

Introduction

After a tremendous number of scientists from different fields dived into the nanoscale world, nanoobjects of different shapes and dimensions have been obtained including the filamentary nanocrystals which are now known as nanowires (NWs). These structures were originally called whiskers due to their whisker-like morphology namely their high length to diameter ratio. Despite of the fact that NWs sometimes used to be considered an unfavourable growth defect, NWs became increasingly popular. Today NW research takes a leading position in nanotechnology.

Such research interest is inextricably linked to a number of unique properties offered by NWs, such as self-assembly and organization, integration of NW-based devices on silicon substrates, the possibility of growth of NW-based non-planar heterostructures and opportunities to control their morphology, composition, optical and electronic properties. For example, NW-based solar cells [1], photodetectors [2], biosensors [3], resonant tunnelling diodes [4] have been demonstrated. Moreover, NWs are very promising for many other applications including the development of quantum computers [5].

Due to a large number of processes occurring during the growth, NW growth remains a "black box". A single model combining all the steps, such as homogeneous and heterogeneous reactions, heating and movement of precursors and processes on the surface still does not exist. Models are still based on rate-limiting steps (kinetics, thermodynamics and mass transport). Fortunately, the composition, stoichiometry, doping, growth rate and morphology can often be described independently. However, the governing equations are sometimes so difficult that an analytical solution is not possible and numerical calculations are required.

This licentiate thesis is devoted to the theoretical study of the composition and crystal phase of ternary semiconductor NWs. Firstly, the model of the formation of a ternary nucleus from a quaternary liquid melt through calculation of the chemical potential difference between solid and liquid states has been developed.

Then, this model has been used for modelling the crystal phase of a ternary NW. The phase control has been considered for the example of InGaAs NWs. However, this model can be easily applied to any ternary materials system. It should be noted that within the model the composition of the growing monolayer is the same as the composition of the nucleus, i.e. the macroscopic composition is completely determined by thermodynamics and coincides with the nucleus composition. However, the NW composition may also be influenced by the incorporation rate of adatoms to the perimeter of the growing monolayer. In this case kinetic modelling is required. At such conditions compositions within the miscibility gap can be obtained [6].

The structure of this licentiate thesis is the following. In the second chapter the most important NW growth methods are considered. This chapter includes a brief description of the vapor-liquid-solid mechanism (VLS), foreign metal catalyzed, self-catalyzed and self-induced growth, selective area epitaxy, molecular beam epitaxy and metal organic chemical vapor deposition. In the third chapter the basics of thermodynamics required for NW growth modelling are presented. Special attention is paid to the Gibbs free energy, chemical potentials, driving force and nucleation. Finally, the fourth chapter is devoted to ternary NWs, the formation of a miscibility gap and the zinc blende (ZB) and wurtzite (WZ) crystal structures.

Chapter 2

Brief history and description of nanowire growth

Growth of NWs was first reported by Wagner and Ellis in 1964 [7]. Within the experiment $SiCl_4$ molecules were deposited on a Si substrate with gold droplets. These droplets play the role of collection sites of semiconductor materials (Si atoms). Catalyst droplets are used today to reduce the growth temperature and activation energy of the nucleation process. A relatively large concentration of Si leads to a supersaturation resulting in nucleation and growth. The growth occurs under the gold droplets only (here we ignore possible parasitic growth). This way of formation is known as the VLS mechanism due to the three phases involved in the growth.

Afterwards, the research interest has been focused on VLS growth of III-V NWs. The shift to usage of group III elements as a catalyst instead of a foreign metal catalyst, such as Au [8,9], allowed to avoid NW contamination and degradation of their optoelectronic properties [10]. This growth method called self-catalyzed growth became a real breakthrough [11-13]. So, self-catalyzed growth goes beyond foreign metal catalyzed growth in morphology control of NWs due to the self-focusing effect [14,15]. The effect is that NW radii converge to a certain radius during growth because of different radius dependence of atomic fluxes. Thus, the self-focusing effect enables the growth of a NW array with a high degree of uniformity of the NW diameters despite of the initial droplet size distribution. That is in contradiction to foreign metal catalyzed growth where the NW radius is predominantly determined by the radius of the foreign metal catalyst droplet [16].

The next step forward is selective area epitaxy which is growth of NWs on a patterned substrate [17,18]. For this an amorphous layer (often SiN_x or SiO_x) is deposited on the substrate. Then holes, or the windows, are opened using lithography and etching. As a result, nanostructures grow selectively in these windows while no growth occurs on the mask since the deposited materials do not stick on the amorphous mask. This growth technique allows to study the influence

of individual growth parameters on NW growth, for instance the influence of pitch (the separation between the mask openings) which can modify the effective diffusion length of adatoms [19].

Finally, it is possible to grow a NW without a catalyst droplet. This method is called self-induced growth and very important for growth of GaN NWs for instance [20,21]. In contrast to VLS growth, group III elements are not in excess anymore. That is why it is necessary to consider the growth (the growth rate) in terms of both group III and V elements through the probability for them to meet and incorporate into a growing monolayer [22]. The main challenge of self-induced growth is to find growth conditions that favor anisotropic NW growth instead of 2D layer growth (epitaxial lateral overgrowth).

Molecular beam epitaxy (MBE) was developed in the late 1970s by J.R. Arthur and A.Y. Cho and is one of the most popular and advanced growth technique. This process consists of deposition of semiconductor materials in ultra-high vacuum conditions (10^{-8} – 10^{-12} Torr) with beams of atoms or molecules [23]. The MBE process is characterized by an absence of homogeneous reactions in the growth chamber and high control of growth parameters such as purity of sources, precise flux ratio, and a quick beam flux switch which is not available for other techniques. This results in perfectly abrupt interfaces, high degree of crystallinity and high uniformity of NW arrays. The precise control and a relatively low growth rate makes this method the best for growth of NW-based heterostructures which are required for fabrication of solar cells, lasers and single photon sources. The negative aspect is the complexity and high cost of growth equipment and service (semiconductor sources and substrates).

Another epitaxial technique widely used to grow NWs is metal organic vapor phase epitaxy (MOVPE) [24]. The MOVPE growth process involves the pyrolysis of organometallic precursor molecules, which makes the chemistry of the process very complicated. The typical pressures are in the range of 10 to 760 Torr and a carrier gas, most often hydrogen, is used to carry the precursors to the growth front. MOVPE is cheaper than MBE and gives higher growth rates. However, most gases, especially, the group V precursors are very toxic.

Hydride vapor-phase epitaxy (HVPE) has become very popular in the fabrication of AlN, GaN, GaAs, InP semiconductors due to a fast growth rate and the low cost of synthesis [25]. As the name implies, the group V element are transported using hydrides (AsH_3, PH_3, or NH_3). The group III precursors are chlorides.

Chapter 3

Thermodynamics

3.1 Thermodynamic functions and equilibrium

Thermodynamic modelling helps to understand NW growth. Even if kinetics can play a major role, thermodynamics allows to describe some of the processes that occur during growth and to estimate optimal growth conditions, including temperature, pressure, total amount and ratio of species.

From the perspective of thermodynamics, the growth process occurs in an open system where the composition and amount of matter change. When optimal growth conditions are found and set up, temperature and pressure can be considered as constants. In such circumstances, it is convenient to describe changes in the state of a system in terms of the Gibbs free energy:

$$dG = VdP - SdT + \sum_i \mu_i dn_i. \quad (1)$$

Here G is the Gibbs free energy, T is temperature, S is entropy, V is volume, P is pressure, μ_i is the chemical potential of the species i and n_i is particle number of species i.

Other thermodynamic quantities can be derived from the Gibbs free energy, including entropy, enthalpy H, volume, heat capacity, thermal expansion, isothermal compressibility and, the most important, the chemical potential. The chemical potential of the component *i* is the partial derivative of the Gibbs free energy with respect to the amount of the *i* species, while pressure, temperature and all other species' concentrations in the mixture remain constant:

$$\mu_i = \left(\frac{\partial G}{\partial n_i}\right)_{P,T,n_j} \quad (2)$$

The physical meaning of the chemical potential is the change of the Gibbs free energy of a homogeneous multicomponent system upon adding one mole of a certain component at constant pressure, temperature and system composition.

Moreover, chemical potentials can be defined based on any one of the energy state functions,

$$\left(\frac{\partial U}{\partial n_i}\right)_{S,V,n_j}, \quad \left(\frac{\partial H}{\partial n_i}\right)_{S,P,n_j}, \quad \left(\frac{\partial F}{\partial n_i}\right)_{T,V,n_j}, \quad \text{or} \quad \left(\frac{\partial G}{\partial n_i}\right)_{P,T,n_j}, \tag{3}$$

where F is the Helmholtz free energy and U is the internal energy. However, only the last one, based on G, is a partial molar property.

In relation to nanostructure growth, one of the most fundamental purposes of thermodynamics is to provide the relationship which would link the compositions of the various phases that are in contact with each other in an equilibrium system at constant temperature and pressure. A phase is a domain within which all relevant properties of a thermodynamic system such as chemical composition, stoichiometry and density, are uniform. Two or more phases are in equilibrium if a set of conditions is fulfilled, namely there are equalities of temperatures (thermal equilibrium), pressures (mechanical equilibrium) and chemical potentials (chemical equilibrium). The Gibbs free energy of the system at equilibrium has a minimum value (alternatively, the entropy is maximized).

3.2 Driving force

Let's us consider an isolated system composed of the phases α and β. Fig. 1 shows the qualitative temperature dependence of the chemical potentials μ_α and μ_β. As seen in Fig. 1, the two curves cross at temperature T_e which is the equilibrium temperature. The phase β has the lower chemical potential in the temperature region below T_e whereas the phase α has a lower chemical potential at higher temperatures. Thus the decrease of the temperature from T_a to T_b will lead to the phase transition from α to β.

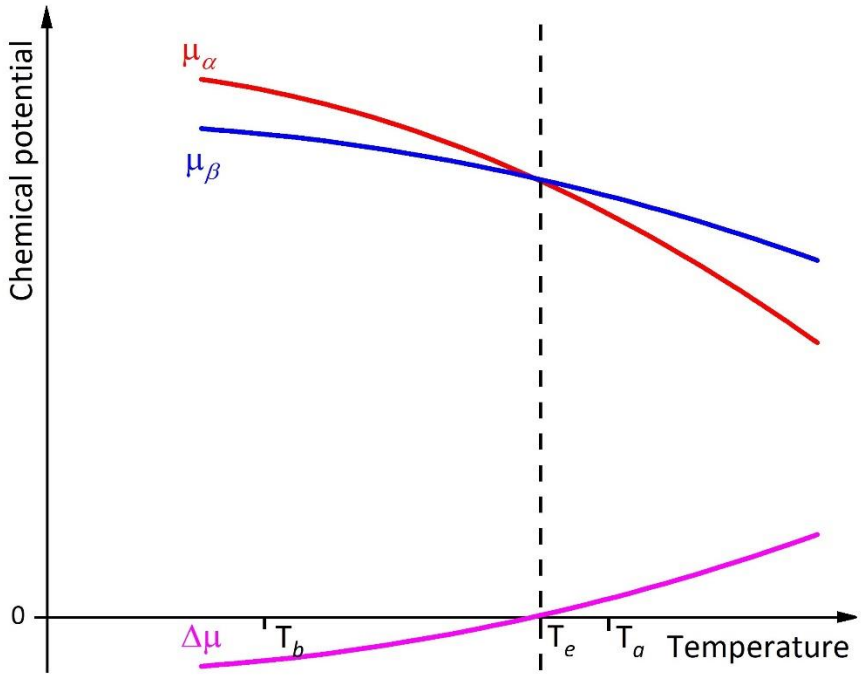

Figure 1. Temperature dependence of the chemical potentials and the difference of the chemical potentials.

Applying this to NW growth via the VLS mechanism, crystallization occurs from a solution which is a catalyst liquid alloy droplet. Then, the difference in the chemical potential between the initial state μ_i and the final state which is at the equilibrium chemical potential μ_e is called the driving force and can be written as:

$$\Delta\mu = \mu_i - \mu_e \tag{4}$$

The driving force for an ideal solution (a dilute metastable system) can be expressed as

$$\Delta\mu = k_B T ln\frac{n}{n_e} = k_B T ln(\zeta + 1) \tag{5}$$

Here, n is the concentration in a metastable phase and n_e is the corresponding equilibrium concentration. The term $\zeta = n/n_e - 1$ is called the supersaturation.

3.3 Models of Gibbs free energy

Before doing any thermodynamic calculations, it is necessary to find the analytical expressions of the Gibbs free energy of all phases.

In the general case, the Gibbs free energy of a multicomponent system composed of N components (solid or liquid solution) is given by

$$G(T, x_i) = \sum_i x_i G_i^0 - TS^m + G^{ex} \tag{6}$$

Here, the first term is the sum of the Gibbs free energies of the pure elements G_i^0 with x_i the mole fraction of component i as weight. The second term describes the configurational entropy S^m. Assuming uniform distribution of species over the whole volume of the phase (the components are randomly mixed), the entropy of mixing can be obtained in the next form:

$$S^m = -k_B \sum_i x_i ln x_i \tag{7}$$

The first two terms correspond to the case of an ideal solution, i.e. a solution in which the enthalpy of mixing is zero.

When the enthalpy of mixing is non-zero, deviation from ideal solution behaviour is described by the excess Gibbs energy G^{ex} which is the third term in eq. 6. Such deviation arises from different interactions between the mixture components. The excess Gibbs energy can be expressed as the sum of the binary excess Gibbs energy G_{bin}^{ex} due to binary interactions, the ternary excess Gibbs energy G_{bin}^{ex} due to ternary interactions and higher order excess energy G_h^{ex}:

$$G^{ex} = G_{bin}^{ex} + G_{ter}^{ex} + G_h^{ex} \tag{8}$$

The binary and ternary excess Gibbs energies of a solution have the following form

$$G_{bin}^{ex} = \sum_{i=1}^{N-1} \sum_{j>i}^{N} x_i x_j \omega_{ij} \tag{9}$$

$$G_{ter}^{ex} = \sum_{i=1}^{N-2} \sum_{j>i}^{N-1} \sum_{k>j}^{N} x_i x_j x_k \omega_{ijk} \tag{10}$$

Here x_v is the molar fraction of the element ($v = i, j, k$) and ω_{ij} and ω_{ijk} are the binary and ternary interaction parameters. Within the Redlich-Kister model, the interaction parameters can be expressed as:

$$\omega_{ij} = \sum_{v=0}^{k} (x_i - x_j)^v \omega_{i,j}^v \tag{11}$$

$$\omega_{ijk} = (x_i + \delta_{ijk})\omega_{i,j,k}^i + (x_j + \delta_{ijk})\omega_{i,j,k}^j + (x_k + \delta_{ijk})\omega_{i,j,k}^k \tag{12}$$

where $\delta_{ijk} = (1 - x_i - x_j - x_k)/3$, parameters $\omega_{i,j}^v$ and $\omega_{i,j,k}^v$ are temperature-independent or linear-dependent on the temperature and can be obtained from the parameter optimization in accordance with experimental data.

Usually, it is enough to present $\omega_{i,j}^v$ and $\omega_{i,j,k}^v$ as a linear temperature dependent parameters

$$\omega_{i,j}^v = a_{ij}^v + b_{ij}^v T \tag{13}$$

$$\omega_{i,j,k}^v = a_{ijk}^v + b_{ijk}^v T \tag{14}$$

with a_{ij}^v, b_{ij}^v, a_{ijk}^v and b_{ijk}^v being constants.

Accounting for binary and ternary interactions is necessary for the correct description of multicomponent systems, whereas higher-order terms generally can be ignored in thermodynamic computations.

In the case of a ternary solid solution $A_xB_{1-x}D$, the enthalpy of mixing is described by the pseudobinary interaction parameter ω_s (which can be composition-dependent), that is, according to eq. 11 $\omega_s = \omega_s^0 + \omega_s^1(2x - 1)$:

$$\Delta H = x(1 - x)\omega_s \tag{15}$$

3.4 Nucleation

It is widely established that NW growth occurs as a result of a nucleus forming and its subsequent growth into a 2D layer [26]. Normally, the growth time (the time needed to complete a monolayer) is shorter than the time between two nucleation events. As a result, a NW grows in the layer-by-layer regime. However, the preferential nucleation site could be at the triple line (the edge of the growth interface, where all the three phases meet) or in the center of the growth interface, depends on the growth conditions [27].

In the general case, the change of Gibbs energy associated with the nucleus formation is given by

$$\Delta G = -\Delta\mu s + \Gamma P_n h + \gamma_{LV}\Delta A \quad (16)$$

Here $\Delta\mu$ is the chemical potential difference between the liquid particle and the solid nucleus and s is the number of III-V pairs in the nucleus, Γ is the effective surface energy, P_n is nucleus perimeter and h is layer height. The first term describes the energy released by increasing the volume of the nucleus. The second term corresponds to the surface free energy due to creation of an interface between the new phase and the metastable initial phase. The last term is a VLS specific term and refers to the change of the drop surface ΔA due to the island formation where γ_{LV} is the liquid-vapor surface energy.

The size of the critical nucleus and the nucleation rate can be found by minimizing the formation energy. Applying this approach to different crystal structures, we have developed a model for the composition dependence of the WZ-ZB polytypism in ternary NWs growing by the VLS mechanism.

Of course, the composition of the layer can differ from the composition of the nucleus. So, the macroscopic NW composition can be determined by kinetics. However, in the current work we limit ourselves to consideration of the nucleation-limited growth regime. The combination of thermodynamic and kinetic models could indeed be an interesting future problem.

Chapter 4

Ternary nanowires: miscibility gap and crystal structure

4.1 Ternary nanowires

The ability to grow ternary solid solutions (structures composed of two binary semiconductors which have the same cation or anion) have opened new horizons [28-30]. Discrete bandgap values of elemental and binary compound semiconductors have been replaced by the possibility to choose the required one from a continuous range of values [31]. This is possible due to the change of proportion between two binary semiconductors in a solution, or simply put, varying the solid composition. The solid composition primarily depends on the vapor phase composition and growth temperature.

The lattice parameter of a ternary solid solution $A_xB_{1-x}D$ is approximately a weighted mean of the two constituents lattice parameters at the same temperature:

$$a_{\mathrm{A_xB_{1-x}D}} = x a_{\mathrm{AD}} + (1-x) a_{\mathrm{BD}} \tag{17}$$

Here, a_{AD} and a_{BD} are the lattice parameters of the AD and the BD binary semiconductors respectively. This equation is known as Vegard's law.

In many binary semiconductor systems, the band gap is approximately also a linear function of the lattice parameter. Then the band gap of the ternary solid solution $E_{\mathrm{g,AxB1-xD}}$ can be calculated by means of Vegard's law

$$E_{\mathrm{g,AxB1-xD}} = x E_{\mathrm{g,AD}} + (1-x) E_{\mathrm{g,BD}} \tag{18}$$

Here, $E_{\mathrm{g,AD}}$ and $E_{\mathrm{g,BD}}$ are the band gaps of the AD and the BD binary semiconductors respectively.

Besides of bandgap tuning, a number of properties of the final structure changes with the composition, such as the lattice parameter, the density of states and the optical properties.

However, not all solid compositions are thermodynamically stable during growth. So, at some concentrations, the growth of domains composed of pure binary compounds is more energetically favourable. Thus, at such conditions, the formation of a homogeneous ternary solid solution is thermodynamically forbidden. In spite of the fact that in the macroscopic point of view the average composition will be as it is required, the real optical and electronic properties will significantly differ being some combination of binary compounds. It reduces the structure quality and the efficiency of the final NW-based device. This range of the forbidden compositions is called the miscibility gap and is observed in structures of different dimensions including bulk structures, thin films and NWs [32]. By growing the material far from thermodynamic equilibrium, even compositions within the miscibility gap can be reached.

A theoretical investigation of the composition control based on thermodynamic considerations, namely the influence of the liquid composition of the droplet on the NW solid composition is presented in Paper 1.

4.2 Binodal and spinodal

In the classical nucleation theory, two characteristic curves, namely the binodal and spinodal, play an important role. The binodal separates the single-phase state region from a region where two distinct phases may coexist. The binodal which separates the homogeneous solid solution from the miscibility gap region is called solvus. In order to find it, it is necessary to calculate the derivative of the Gibbs free energy of with respect to solid composition x and equate the result to zero. So, within the regular solution model ignoring possible composition-dependent parameters, the binodal (solidus in this case) can be written in the form

$$T_b = \frac{\omega_s(1-2x)}{Rln\frac{1-x}{x}} \tag{19}$$

with R being the gas constant.

The second curve, the spinodal, represents the limit of absolute instability between phases. It is defined by the condition that the second derivative of Gibbs free energy is zero and takes the form

$$T_s = \frac{2\omega_s}{R} x(1-x) \tag{20}$$

It can be noticed that the spinodal is always under the binodal except of the critical point in the center where they meet.

An example of the binodal and spinodal lines for the ternary AlInAs materials system calculated using eq. 19 and 20 is presented in Fig. 2.

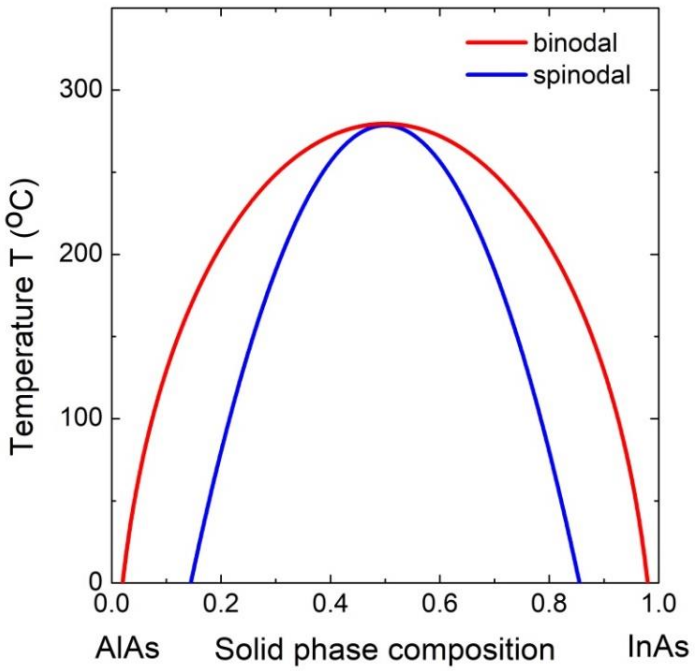

Figure 2. The binodal and spinodal lines calculated for ternary AlInAs materials system [33].

The composition above the binodal corresponds to stable state of a homogeneous solid solution. The region between the binodal and spinodal lines corresponds to a metastable state: the homogeneous solid solution can persist at small enough fluctuations. Finally, under the spinodal line arbitrarily small fluctuations in the system lead to phase separation via the so called spinodal decomposition mechanism.

Thus, NWs with composition within the miscibility gap region can be grown. Such compositions are thermodynamically unstable while we will focus on the thermodynamically stable states in this contribution.

As can be seen in eq. 19, the pseudo-binary interaction parameter is a key parameter which defines the width of the miscibility gap region: the larger its value, the bigger the miscibility gap and the higher the critical temperature, above which the miscibility gap vanishes (Paper 1).

Accounting for the second Redlich–Kister polynomial parameter, i.e. introducing composition-dependent terms, leads to an asymmetrical shape of the miscibility gap.

4.3 Crystal structure

As is widely known, III-V NWs can be composed of different crystal structures [34]. This phenomenon being a topic of comprehensive research is called polytypism. Incorrectly chosen conditions or the change of growth conditions can lead to formation of a NW which may combine different crystal structures. This unwanted and uncontrollable alternation of crystal structures destroys the crystal symmetry resulting in appearance of local potentials which can act as centers of nonradiative recombination for instance. Crystal phase engineering (controllable switching between different crystal structures) can be achieved by varying the growth conditions: the flux ratio and temperature.

Crystal structures of ZB and WZ are presented in Fig. 3. From the thermodynamic point of view, the energy difference between crystal structures can be described by the difference in the cohesive energy. This is the energy needed in order to rip a sample apart into a gas of widely separated atoms.

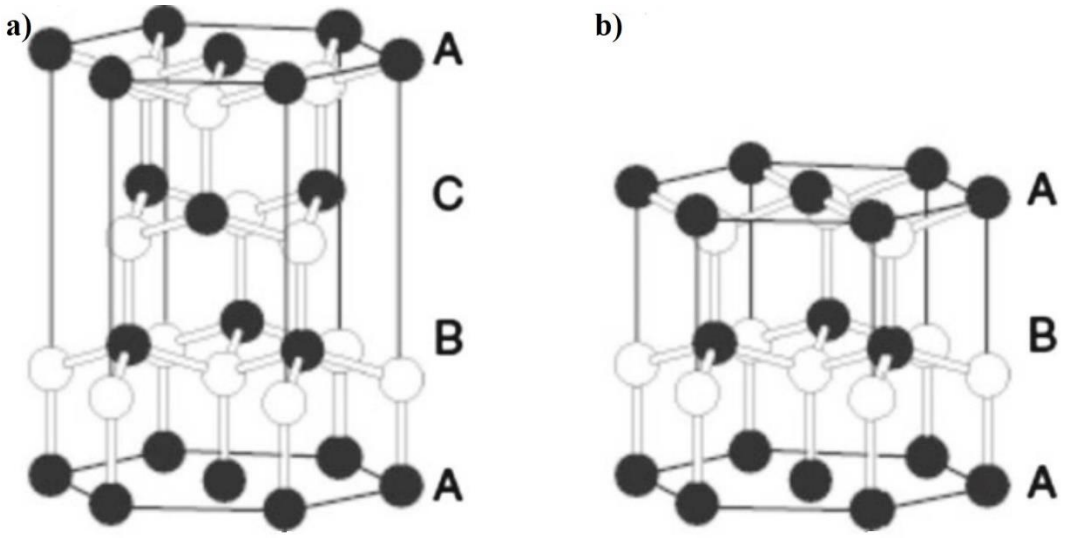

Figure 3. ZB (a) and WZ (b) crystal structures [35].

The selection of crystal structure during growth is defined by the chemical potentials and depends on the V/III flux ratio and the contact angle [27]. The details of our investigation can be found in Paper 2. There we calculate the probability of the formation of the ZB and WZ structures. Despite the fact that several parameters are still unknown, Paper 2 is a useful tool for modelling and understanding of the crystal phase formation in ternary NWs. Modern *in -situ* measurement methods allows to get a look into the processes occurring during the growth [36]. Recently, an astonishing progress has been made in crystal phase engineering: structures with atomically controllable crystal phase superlattices have been grown and presented by Dick [37].

Chapter 5

Summary and outlook

To summarize, the composition and crystal structure of ternary nanowires nucleating from quaternary liquid melts have been studied by theoretical models.

First, an analytic expression for the composition of a ternary III-V NWs as a function of the liquid droplet composition has been derived. The core of the model is two-component heterogeneous nucleation. The distinguishing feature is that numerous interactions occurring during VLS growth from a quaternary liquid melt are taking into account, including composition dependent interaction parameters. In-Ga-As-Au, Al-Ga-As-Au, In-Ga-Sb-Au and In-Sb-As-Au materials systems have been considered and discuss in detail. It has been found that the composition of $Al_xGa_{1-x}As$ can be varied over a wide range of the droplet composition. However, for several materials systems such as $In_xGa_{1-x}Sb$ and $In_xGa_{1-x}As$, composition tuning is limited by a large miscibility gap. The reason for the forbidden composition-range is a high value of the pseudobinary interaction parameter. In any case, composition tuning over a wide range requires a very high concentration ratio in the droplet. The comparison of the analytical expression with the numerical calculation showed the proximity of results. Putting the foreign catalyst concentration to zero, the model has been adapted to describe self-catalyzed growth. In spite of lack of data about the droplet composition, the obtained model gives insights into the composition tuning of ternary nanowires.

Next, based on the previous model, a model which allows to describe ZB-WZ polytypism has been developed by introducing the difference in the cohesive energy between the ZB and WZ structures. To do so, the probabilities of nucleus formation of both ZB and WZ structures at the triple line or in the center of the growth interface have been calculated using the example of $In_xGa_{1-x}As$ NWs. The obtained theoretical results are in good agreement with available experimental data.

Both models can be easily applied to other ternary and quaternary materials systems.

There are several directions for future investigations in this topic. First, it is the thermodynamic assessment of the Gibbs free energies and interaction parameters of new ternary and quaternary materials systems. Then the obtained values can be used for NW growth modelling. Next, the combination of thermodynamic and kinetic models is an interesting research problem. So, one may link the composition of the vapor and the liquid droplet through kinetics and combine it with the described thermodynamic model to get a vapor-solid model. Third, the thermodynamic model can be used for the modelling of heterostructure interfaces in NWs. Finally, finding a more accurate form for the difference in the cohesive energy between ZB and WZ is of great importance for the modelling crystal structure of NWs.

Bibliography

[1] A. Kandala, T. Betti and I. M. Fontcuberta, *Phys. Status Solidi*, 2009, **1**, 173

[2] X. Dai, S. Zhang, Z. Wang, G. Adamo, H. Liu, Y. Huang, C. Couteau, and C. Soci, *Nano Lett*., 2014, **14** (5), 2688

[3] E. Patolsky, G. Zheng, O. Hayden, M. Lakadamyali, X. Zhuang, C. M. Lieber, *Proc. Acad. Sci. USA*, 2004, **101**, 14 017

[4] G. Zheng, W. Lu, S. Jin and C. M. Lieber, *Adv. Mater*., 2004, **16**, 1890

[5] S. Gazibegovic, D. Car, H. Zhang, S. C. Balk, J. A. Logan, M. W. A. de Moor, M. C. Cassidy, R. Schmits, D. Xu, G. Wang, P. Krogstrup, R. L. M. Op het Veld, K. Zuo, Y. Vos, J. Shen, D. Bouman, B. Shojaei, D. Pennachio, J. S. Lee, Petrus J. van Veldhoven, S. Koelling, M. A. Verheijen, L. P. Kouwenhoven, C. J. Palmstrøm and E. P. A. M. Bakkers, *Nature*, 2017, **548**, 434–438

[6] A. Ameruddin, H. A. Fonseka, P. Caroff, J. Wong-Leung, R. LM Op het Veld, J. L. Boland, M. B. Johnston, H. H. Tan and C. Jagadish, *Nanotechnology*, 2015, **26**, 205604

[7] R. S. Wagner and W. C. Ellis, *Appl. Phys. Lett.*, 1964, **4**, 89

[8] Z. H. Wu, X. Y. Mei, D. Kim, M. Blumin, and H. E. Ruda, *Appl. Phys. Lett.*, 2002, **81**, 5177

[9] N. Jiang, J. Wong-Leung, H. J. Joyce, Q. Gao, H. H. Tan, C. Jagadish, *Nano Lett*. 2014, **14 (10)**, 5865-5872

[10] G. Bemski, *Phys. Rev*. 1958, **111**, 1515

[11] C. Colombo, D. Spirkoska, M. Frimmer, G. Abstreiter and A. Fontcuberta i Morral, *Phys. Rev. B: Condens. Matter Mater. Phys*., 2008, **77**, 155326

[12] F. Jabeen, V. Grillo, S. Rubini and F. Martelli, *Nanotechnology*, 2008, **19**, 275711

[13] S. Plissard, K. A. Dick, G. Larrieu, S. Godey, A. Addad, X. Wallart and P. Caroff, *Nanotechnology*, 2010, **21**, 385602

[14] V. G. Dubrovskii, *Phys. Rev. B*, 2016, **93**, 174203

[15] V. G. Dubrovskii, T. Xu, A. Díaz Álvarez, S. R. Plissard, P. Caroff, F. Glas and B. Grandidier, *Nano Lett.*, 2015, **15**, 5580−5584

[16] M. Tchernycheva, L. Travers, G. Patriarche, J. C. Harmand, G.E. Cirlin, V. G. Dubrovskii, *J.Appl. Phys*., 2007, **102**, 094313
[17] A. M. Munshi, D. L. Dheeraj, V. T. Fauske, D. C. Kim, J. Huh, J. F. Reinertsen, L. Ahtapodov, K. D. Lee, B. Heidari, A. T. J. van Helvoort, B. O. Fimland and H. Weman, *Nano Lett.,* 2014, **14(2)**, 960-966
[18] H. Küpers, R. B. Lewis, A. Tahraoui, M. Matalla, O. Krüger, F. Bastiman, H. Riechert and L. Geelhaar, *Nano Res.*, 2018, **11(5)**, 2885–2893
[19] E. D. Leshchenko, P. Kuyanov, R. R. LaPierre and V. G. Dubrovskii, *Nanotechnology*, 2018, **29**, 225603
[20] M. T. Björk, H. Schmid, C. M. Breslin, L. Gignac and H. Riel, *J. Cryst. Growth,* 2012, **344**, 31−37
[21] T. Schumann, T. Gotschke, F. Limbach, T. Stoica and R. Calarco, *Nanotechnology*, 2011, **22**, 095603
[22] V. G. Dubrovskii, *ACS Omega*, 2019, **4**, 8400−8405
[23] A. Fontcuberta i Morrala, C. Colombo and G. Abstreiter, *Appl. Phys. Lett.,* 2008, **92**, 063112
[24] K. Ikejiri, J. Noborisaka, S. Hara, J. Motohisa, T. Fukui, *J. Cryst. Growth*, 2007, **298**, 616−9
[25] E. Gil, Y. André, R. Cadoret, A. Trassoudaine, Hydride VPE for current III-V and nitride semiconductor compound issues, Handbook of Crystal Growth, Vol. III, Second Edition, Elsevier, 2015, Chapter 2, 51-93
[26] D. Jacobsson, F. Panciera, J. Tersoff, M. C. Reuter, S. Lehmann, S. Hofmann, K. A. Dick and F. M. Ross, *Nature*, 2016, **531**, 317–322
[27] F. Glas, J. C. Harmand and G. Patriarche, *Phys. Rev. Lett.*, 2008, **99**, 146101
[28] G. Priante , F. Glas , G. Patriarche , K. Pantzas , F. Oehler and J.-C. Harmand, *Nano Lett*., 2016, **16** , 1917 -1924
[29] C. S. Jung , H. S. Kim , G. B. Jung , K. J. Gong , Y. J. Cho , S. Y. Jang , C. H. Kim , C. W. Lee and J. Park , *J. Phys. Chem. C*, 2011, **115**, 7843 - 7850
[30] L. Li, D. Pan, Y. U. Xue, X. Wang, M. Lin, D. Su, Q. Zhang, X. Yu, H. So , D. Wei, B. Sun, P. Tan, A. Pan and J. Zhao, *Nano Lett.*, 2017, **17**, 622 - 630
[31] C.-Z. Ning, L. Dou and P. Yang, *Nat. Rev. Mater.*, 2017, **2**, 17070
[32] H. Ohtani, K. Kojima and K. Ishida and T. Nishizawa, *J. Alloys Compd.*, 1992, **182**, 103-114

[33] E. D. Leshchenko, V. G. Dubrovskii, J. Johansson, *J. Phys.: Conf. Ser*., 2019, **1199**, 012022
[34] D. Spirkoska, J. Arbiol, A. Gustafsson, S. Conesa-Boj, F. Glas, I. Zardo, M. Heigoldt, M.H. Gass, A.L. Bleloch, S. Estrade, M. Kaniber, J. Rossler, F. Peiro, J.R. Morante, G. Abstreiter, L. Samuelson, A.F.I. Morral, *Phys. Rev. B*, 2009, **80**, 24325
[35] V. G. Dubrovskii, Nucleation theory and growth of nanostructures, Springer, 2014
[36] J. C. Harmand, G. Patriarche, F. Glas, F. Panciera, I. Florea, J.-L. Maurice, L. Travers and Y. Ollivier, *Phys. Rev. Lett*., 2018, **121**, 166101
[37] K.A. Dick, C. Thelander, L. Samuelson, P. Caroff, *Nano Lett.*, 2010, **10** 3494-3499

Paper I

Volume 20 | Number 12 | 28 March 2018 | Pages 1605–1748

CrystEngComm

rsc.li/crystengcomm

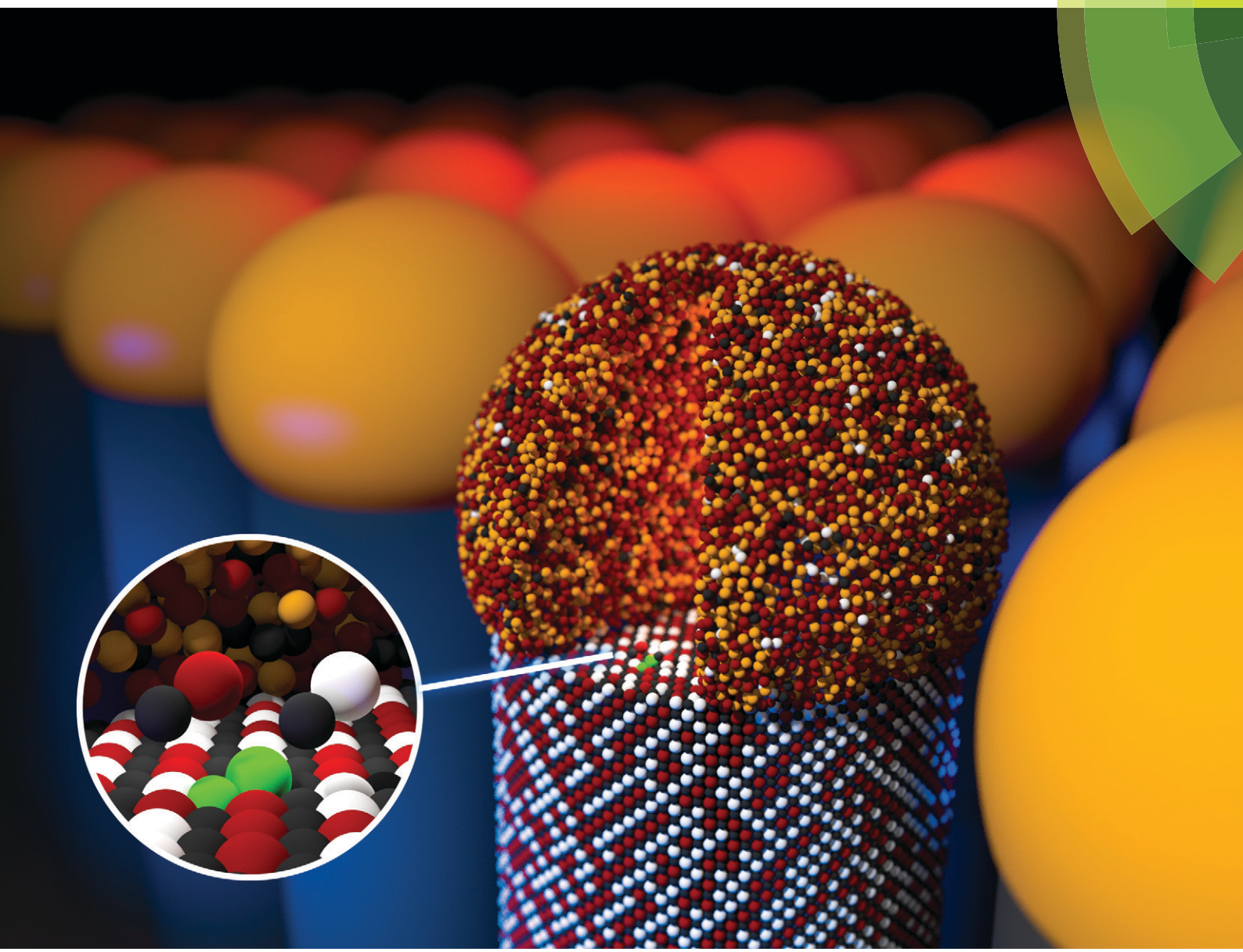

ROYAL SOCIETY OF CHEMISTRY

PAPER

Jonas Johansson *et al.*

Nucleation-limited composition of ternary III–V nanowires forming from quaternary gold based liquid alloys

CrystEngComm

PAPER

View Article Online
View Journal | View Issue

Cite this: *CrystEngComm*, 2018, **20**, 1649

Nucleation-limited composition of ternary III–V nanowires forming from quaternary gold based liquid alloys†

Egor D. Leshchenko,[a] Masoomeh Ghasemi,[ab] Vladimir G. Dubrovskii[c] and Jonas Johansson *[a]

Received 21st December 2017,
Accepted 16th February 2018

DOI: 10.1039/c7ce02201h

rsc.li/crystengcomm

We derive an analytic expression for the composition of a ternary solid material nucleating from a quaternary liquid melt. The calculations are based on the two-component nucleation theory with realistic descriptions of the liquid and solid phases. We apply this theory to gold-catalyzed, nucleation limited vapor–liquid–solid growth of ternary III–V nanowires. We consider ternary gallium, indium, and aluminum arsenides and antimonides and discuss growth conditions for optimum composition control in these materials. Furthermore, we compare our calculations with the results of an equilibrium thermodynamic model.

Introduction

Semiconductor nanowires (NWs) present a promising class of nanoscale objects whose properties are dramatically different from the bulk counterparts. Inspired by the enhanced functionality, III–V NWs have received tremendous research interest[1–3] that led to development of new applications. Particularly, NWs can be used as basic functional elements for a wide range of electronic and optical devices including high brightness light emitting diodes,[4] transistors,[5] low cost solar cells,[6] flexible panel displays,[7] and logic gates.[8] However, applying NW devices to industrial scale requires advanced growth technology with a precise control of the NW composition, heterojunction properties, morphology, and crystal structure. The vapor–liquid–solid (VLS) mechanism[9] is very promising since it enables growth of size-uniform NW arrays with a high degree of crystal quality. This method involves feeding semiconductor materials into a liquid catalyst droplet from the ambient vapor, which leads to vertical crystal growth as a result of supersaturation in the droplet. Self-catalyzed NW growth is a widely used VLS approach[10–14] allowing one to avoid contamination by foreign metals. However, gold remains one of the most attractive catalysts due to its versatility and simplicity of the control over the NW diameter and position.

The critical step in NW-based device design is the ability to control the composition of ternary III–V NWs, which involves the bandgap tunability by variation of the compound concentrations in the ternary alloy. In recent years, enormous progress has been made toward improving the growth technologies by broadening the spectrum of the NW materials. Particularly, growth of AlGaAs and InGaAs NWs using molecular beam epitaxy (MBE)[15] and metal–organic vapor phase epitaxy (MOVPE)[16] have been studied. Sb-based NWs such as GaAsSb,[17] InAsSb (ref. 18) and InGaSb (ref. 19) are nowadays of particular interest in terms of mid-infrared band gap engineering. In these investigations, growth of ternary NWs over a broad range of compositions has been demonstrated. However, the liquid droplet composition has not been systematically investigated which impedes a direct comparison between experimental and theoretical results. NW synthesis resulting in compositions within the miscibility gap can, for systems where this is relevant, be explained in terms of growth kinetics,[20] whereas the present work is devoted to thermodynamically stable compositions.

Analytical models which link the solid–liquid and solid–vapor compositions have been reported by Dubrovskii *et al.*[21,22] and Glas.[23] However, a full description of ternary NWs that form from quaternary alloys (three NW constituencies and gold) is still lacking because of unknown thermodynamic and kinetic constants such as chemical potentials and crystallization rates of different III–V pairs.

The current investigation is aimed at improving the fundamental understanding of the ternary NW formation from quaternary alloys and is based on realistic thermodynamic descriptions of all the considered phases. In our approach, binary and ternary interactions are taken into account. We calculate and analyze compositional diagrams for highly relevant III–V materials including the In–Ga–As–Au, Al–Ga–As–Au, In–Ga–Sb–Au and In–Sb–As–Au systems. Furthermore, a

[a] *Solid State Physics and NanoLund, Lund University, Box 118, 221 00 Lund, Sweden. E-mail: jonas.johansson@ftf.lth.se*
[b] *Physics Department, Persian Gulf University, Box 7513613817, Booshehr, Iran*
[c] *ITMO University, Kronverkskiy prospekt 49, 197101 St. Petersburg, Russia*
† Electronic supplementary information (ESI) available. See DOI: 10.1039/c7ce02201h

comparison between self-catalyzed and Au-catalyzed NW growth in these materials systems is presented. The obtained results provide a basis for understanding the ternary NW formation and can be useful for choosing the growth conditions to tune the NW composition to the desired values.

Calculations

The formation energy of a binary, or two-component, nucleus can be written as[20,24]

$$F(x,s) = -\Delta\mu(x,y)s + a\sqrt{s}, \tag{1}$$

where s is the size and x is the composition of the nucleus, so that $s = i + j$ and $x = i/(i + j)$, where i and j are the number of pairs of the two binaries that the nucleus consists of. The parameter y is the composition of the mother phase, $\Delta\mu(x,y)$ is the chemical potential difference between the mother and daughter phases, and a is a surface energy term. The composition and the size of the critical nucleus are thus given by the simultaneous solutions to the equations

$$\frac{\partial F}{\partial x} = -\frac{\partial \Delta\mu}{\partial x}s + \frac{\mathrm{d}a}{\mathrm{d}x}\sqrt{s} = 0, \quad \frac{\partial F}{\partial s} = -\Delta\mu + \frac{a}{2\sqrt{s}} = 0 \tag{2}$$

It has been argued, however, that the surface energy of the critical nucleus is at a minimum due to surface segregation effects.[25] This property corresponds to the condition da/dx = 0, which considerably simplifies the calculations and leads to the expression

$$\frac{\partial \Delta\mu}{\partial x} = 0 \tag{3}$$

for the composition of the critical nucleus.

We will consider the formation of a ternary alloy, $A_xB_{1-x}D$, from a quaternary solution mother phase containing A, B, D, and U, where U can be thought of as a solvent, often gold. For this situation, the chemical potential difference of the ternary alloy in the liquid and solid can be expressed as[26]

$$\Delta\mu = x(\mu_A^L + \mu_D^L - \mu_{AD}^S) + (1 - x)(\mu_B^L + \mu_D^L - \mu_{BD}^S), \tag{4}$$

where the superscripts L and S refer to the liquid and solid phases, respectively. In order to express chemical potentials, we need thermodynamic models for the Gibbs free energy of the respective phases. The molar Gibbs free energy of the liquid phase is generally given by

$$G^L = \sum_I c_I\mu_I^0 + RT\sum_I c_I \ln c_I + \sum_I \sum_{J=I+1} c_Ic_J\left[\omega_{IJ} + \omega'_{IJ}(c_I - c_J)\right] + \sum_I \sum_{J=I+1} \sum_{K=J+1} c_Ic_Jc_K\omega_{IJK}, \tag{5}$$

where c_I is the molar fraction of element I in the liquid phase, μ_I^0 is chemical potential of pure component I in the liquid state, R is the gas constant, and T is temperature. The ω are interaction parameters accounting for deviations from ideality. For binary interactions, we assume a sub-regular solution model with composition dependent interactions, whereas the ternary interaction parameters are assumed to be independent of composition. All ω parameters are allowed to be temperature dependent. For the composition dependent binary interactions, one needs to be careful with the order of the indices. In CALPHAD, one uses an alphabetical order convention and writes the composition dependent part of the AB interaction term as $x_Ax_B\omega'_{AB}(x_A - x_B)$. If, for instance, A is interpreted as In and B as Ga, the alphabetical order is broken and we need to construct $\omega'_{InGa} = -\omega'_{GaIn}$, where ω'_{GaIn} is the standard tabulated parameter (because Ga comes before In according to alphabetical order). For the composition independent interaction terms (binary and ternary), the order does not matter.

The chemical potentials of the species in the liquid are expressed by differentiation of G^L in eqn (5) according to

$$\mu_J^L = G^L + \frac{\partial G^L}{\partial c_J} - \sum_I c_I\frac{\partial G^L}{\partial c_I}. \tag{6}$$

The zincblende (ZB) solid phase, $A_xB_{1-x}D$, is modeled as a binary regular solid solution with chemical potentials given by

$$\mu_{AD}^S = \mu_{AD}^0 + RT\ln x + (1-x)^2\left[\omega_S + (4x-1)\omega'_S\right] \tag{7a}$$

$$\mu_{BD}^S = \mu_{BD}^0 + RT\ln(1-x) + x^2\left[\omega_S + (4x-3)\omega'_S\right], \tag{7b}$$

where μ_{AD}^0 and μ_{BD}^0 are the chemical potentials of pure AD and BD binaries, respectively, and ω_S, ω'_S are the temperature dependent interaction parameters of zero and first order.

By explicitly expressing the chemical potentials of the species in the liquid, we construct the chemical potential difference according to eqn (4). Differentiating this expression according to eqn (3) yields an analytical expression for the composition of the critical nucleus, which serves as a first approximation of the composition of the solid phase,

$$RT\ln\left(\frac{x}{1-x}\right) - 2\omega_S\left(x - \frac{1}{2}\right) - \omega'_S(6x^2 - 6x + 1) = \varphi(y). \tag{8}$$

Here, we introduce the $\varphi(y)$ function given by

$$\varphi(y) = \alpha + RT\ln\left(\frac{y}{1-y}\right) - 6c_{tot}^2\omega'_{AB}y^2 - 2c_{tot}\left[\omega_{AB} - 3c_{tot}\omega'_{AB} - c_D(\omega'_{AB} + \omega'_{BD}) - c_U(\omega'_{AU} + \omega'_{BU}) + c_D\omega_{ABD} + c_U\omega_{ABU}\right]y, \tag{9}$$

with

$$\begin{aligned}\alpha = {} & \Delta\mu^0_{AD} - \Delta\mu^0_{BD} + \left(\omega_{AB} - c_{tot}\omega'_{AB} - 2c_D\omega'_{BD} - 2c_U\omega'_{BU}\right. \\ & \left. + c_D\omega_{ABD} + c_U\omega_{ABU}\right)c_{tot} + \left(\omega_{AD} - \omega_{BD}\right)c_D \\ & + \left(\omega_{AU} - \omega_{BU}\right)c_U - \left(\omega'_{AD} - \omega'_{BD}\right)c_D^2 - \left(\omega'_{AU} - \omega'_{BU}\right)c_U^2 \\ & + \left(\omega_{ADU} - \omega_{BDU}\right)c_Dc_U.\end{aligned} \tag{10}$$

In the above equations, we have made the substitutions $c_{tot} = c_A + c_B$ and $y = c_A/c_{tot}$. In some relevant cases (see the discussion in ref. 20 for self-catalyzed growth), there is a closed form approximation for eqn (8) given by

$$y = \frac{x}{x + (1-x)e^{\frac{2\omega_S(x-1/2)+\omega'_S\left(6x^2-6x+1\right)+b}{RT}}}. \tag{11}$$

Here,

$$\begin{aligned}b = {} & \alpha - 6c_{tot}^2\omega'_{AB} \\ & - 2c_{tot}[\omega_{AB} - 3c_{tot}\omega'_{AB} - c_D\left(\omega'_{AD} + \omega'_{BD}\right) - c_U\left(\omega'_{AU} + \omega'_{BU}\right) \\ & + c_D\omega_{ABD} + c_U\omega_{ABU}]\end{aligned} \tag{12}$$

for systems requiring values of y close to one to get any appreciable amount of AB in the solid and

$$b = \alpha \tag{13}$$

for systems with the reversed behavior.

From the thermodynamic point of view, the selected states (c_{tot}, y, c_D and T) of the homogeneous liquid particle are not equilibrium states but rather represent a supersaturation with respect to the ZB solid phase. This does not guarantee that there is no thermodynamic driving force for other solid phases to form. According to the Gibbs phase rule, as many as six phases can coexist in a quaternary system. However, we assume that our system is at a non-equilibrium steady state where only the ZB phase forms from the supersaturated liquid and the formation of other solid phases (if they can exist at the given conditions) is kinetically inhibited. As far as possible, we will choose conditions based on the reported experimental results for the respective systems.

Results and discussion

In this section, we calculate and discuss the compositional diagrams for the four materials systems which are technologically highly relevant. The phase diagrams have been constructed using the Thermo-Calc software.[27] The list of the interaction parameters and the Gibbs energy functions is presented in the ESI.†

We start our investigation with the analysis of gold-catalyzed $In_xGa_{1-x}As$ NWs. The InAs–GaAs pseudobinary interaction parameter is large and gives rise to a significant miscibility gap where the formation of the homogeneous solid solution is thermodynamically forbidden at the relevant growth temperatures. From the GaAs–InAs vertical section of the phase diagram of the In–Ga–As–Au system presented in Fig. 1 (c_{tot} = 0.5 and c_{As} = 0.02), it is seen that the $In_xGa_{1-x}As$ phase exists over the entire range of relevant temperatures. Fig. 2 shows the liquid droplet composition *versus* the $In_xGa_{1-x}As$ solid composition at T = 477 °C and c_{As} = 0.02 in a wide range of the total concentrations of group III elements from c_{tot} = 0.98 (corresponding to self-catalyzed growth without gold) to c_{tot} = 0.3, where gold dominates in the catalyst droplet. It should be noted that, whereas the NW composition can be measured accurately using high-resolution electron microscopy techniques,[17] the composition of the droplet during growth is generally unknown. However, an experimental value of group III elements concentration in the Au–III droplet has been estimated to c_{tot} = 0.5 by Harmand *et al.*[28] The amount of group V elements is very small due to the low solubility of arsenic in Au–III alloys. In spite of its negligible amount, the concentration of group V elements has drastic influence on the chemical potentials and, consequently, on the growth rates and crystal structures of ternary NWs.[29] As seen from Fig. 2, reasonable agreement between our analytical model and a purely thermodynamic phase segregation model (represented by the open circles) is observed. This model is based on segregation of a hypothetical, homogeneous supersaturated liquid with composition y into a solid phase with composition x, and a remaining liquid in equilibrium with the solid phase. The phase segregation data were evaluated using the Thermo-Calc software.

The slope of the $y(x)$ curve is practically vertical over almost the entire y range and changes only for $y > 0.97$. Therefore, very high y values are needed to tune the composition of $In_xGa_{1-x}As$ NWs. As noticed above, a direct comparison between the experimental and theoretical liquid–solid

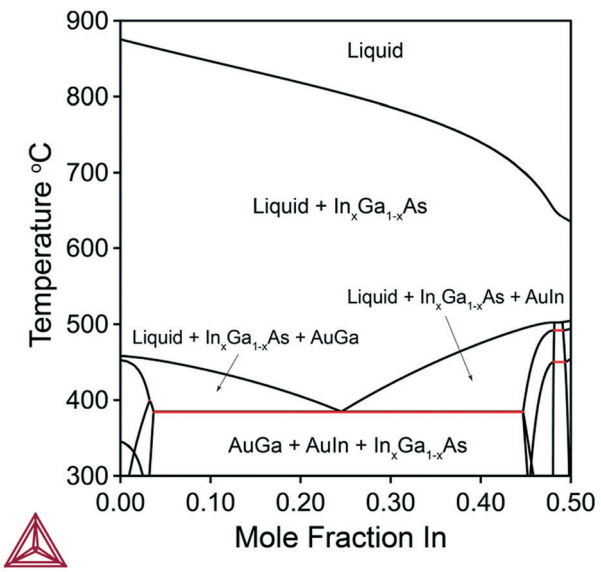

Fig. 1 Vertical section of the In–Ga–As–Au system at c_{tot} = 0.5 and c_{As} = 0.02.

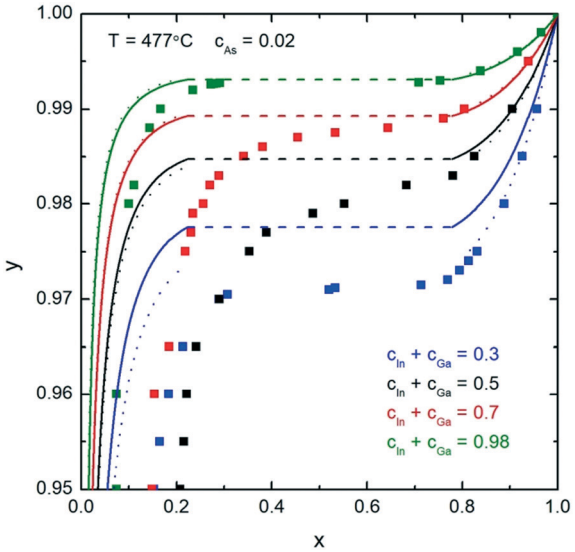

Fig. 2 Analytical calculations (solid curves) for the liquid–solid composition dependence for different c_{tot} at T = 477 °C and c_{As} = 0.02. The dashed parts of the curves correspond to the miscibility gap. The small open circles correspond to phase segregation, evaluated using the Thermo-Calc software. The squares represent results from ref. 24.

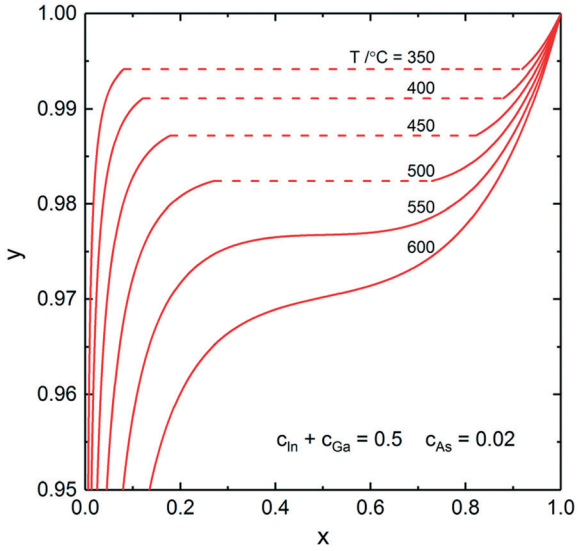

Fig. 3 Analytical calculations (solid curves) for the liquid–solid composition dependence for different temperatures at c_{In} + c_{Ga} = 0.5 and c_{As} = 0.02. The dashed parts of the curves correspond to the miscibility gap.

composition dependences is seriously hampered because of in most cases unknown compositions of the catalyst particles. However, it is possible to describe the main observed trends. So, for example, to synthesize self-catalyzed $In_xGa_{1-x}As$ NWs with x = 0.03–0.05 as obtained in ref. 30, $y \approx$ 0.96–0.98 is required. Moreover, the use of Au catalyst droplets allows one to increase the In fraction up to x = 0.22.[31] This is consistent with the obtained theoretical results: the In fraction in the nanowire decreases with increasing c_{tot} at constant y and T (Fig. 2).

The squares are the numerical results obtained using the previous two-component nucleation model including surface energies and a specific VLS term offsetting the chemical potential difference.[24] The main difference between that nucleation model and the one presented here is that the previous model that includes surface energies admits NW compositions within the miscibility gap. This is because the composition dependent surface energies influence the saddle point coordinates in such a way that it turns the two minima that would correspond to the miscibility gap compositions into one shallow minimum between these two minima.

The relationship between the solid and liquid compositions for different growth temperatures at the fixed c_{tot} = 0.5 is presented in Fig. 3. Clearly, the width of the miscibility gap shrinks with increased temperature and disappears completely at T = 543 °C. This would enable the thermodynamically stable growth of ternary $In_xGa_{1-x}As$ NWs with any x value. However, such high temperatures can be unfeasible for MBE and MOVPE growth due to increased desorption and potential decomposition of III–V materials. Thus, as an example, thermodynamically stable growth of $In_xGa_{1-x}As$ NWs is not possible in the range $0.22 < x < 0.78$ at T = 477 °C (see Fig. 2).

To sum up the results of this section, the required y values for obtaining reasonable InAs fractions in ternary InGaAs NWs increase with the total concentration of group III elements, whereas the III/Au ratio does not change the miscibility gap region which is entirely determined by the temperature-dependent pseudobinary interaction parameter.

Next, we consider nucleation of gold-catalyzed $Al_xGa_{1-x}As$ NWs. Fig. 4a shows a vertical section of the quaternary Al–Ga–As–Au system with c_{tot} = 0.5 and c_{As} = 0.02. While many different phases can be present in the case of Au-assisted NW growth, the $Al_xGa_{1-x}As$ is a dominating solid phase at almost any Au–III ratios and in a wide range of NW growth temperatures. Fig. 4b shows a vertical section of the ternary Al–Ga–As system which is relevant for self-catalyzed growth of $Al_xGa_{1-x}As$ NWs. Fig. 4a reveals that the minimum temperature for Au-catalyzed growth of $Al_xGa_{1-x}As$ NWs should be higher than the eutectic point of the system (T = 353 °C). The minimum VLS growth temperature decreases as the Au concentration decreases. For the $Al_xGa_{1-x}As$ system, the pseudobinary interaction parameter has a low enough value leading to the small dome height in comparison with the $In_xGa_{1-x}As$ system: the critical temperature at which the miscibility gap disappears equals ~142°. This enables the fabrication of $Al_xGa_{1-x}As$ NWs with any solid composition at relevant MBE and MOVPE growth temperatures. The relationship between the solid and liquid compositions for different c_{tot} values at T = 610 °C is presented in Fig. 5. For obtaining self-catalyzed $Al_xGa_{1-x}As$ NWs with non-zero x, very low y values are necessary, while an almost horizontal slope cumbers precise compositional control. Indeed, a small addition of Al to the liquid results in a tremendous increase of the Al concentration in the solid. However, with decreasing c_{tot}, the slope of $y(x)$ changes drastically and the required y values increase by several orders at high enough Au concentrations (c_{tot} = 0.3). The

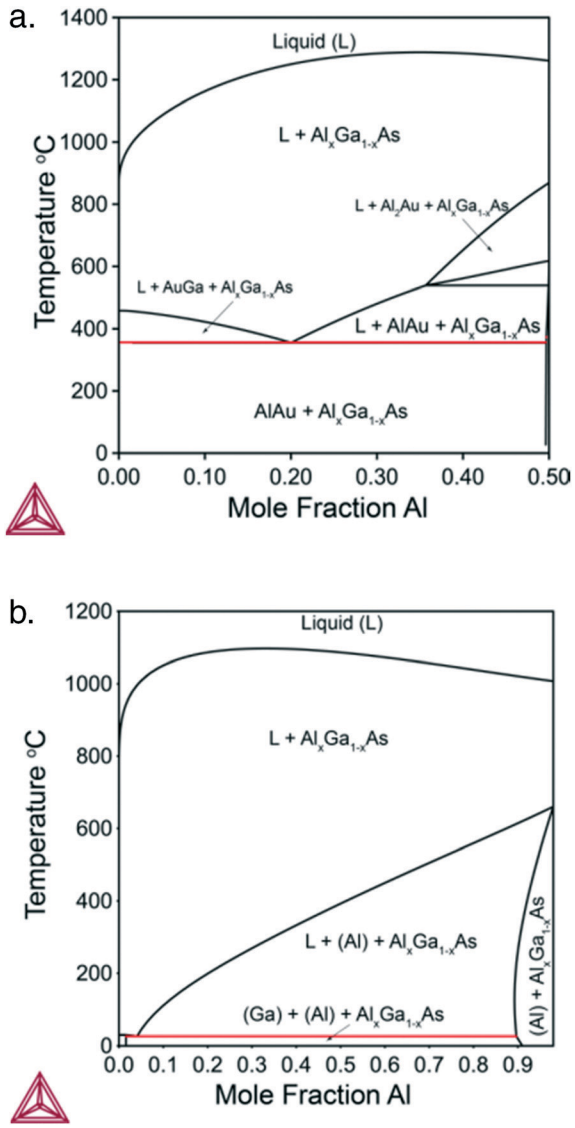

Fig. 4 a. Vertical section of the Al–Ga–As–Au system at c_{tot} = 0.5 and c_{As} = 0.02. b. Vertical section of the Al–Ga–As system at c_{tot} = 0.98 and c_{As} = 0.02.

change of temperature also influences $y(x)$ but not so significant as c_{tot} does. As seen in Fig. 5, the results are well fitted by the one-parametric (ε) Langmuir expression given by $x = \varepsilon y/(1 + y(\varepsilon - 1))$,[15] whereas tremendous discrepancy in comparison to the phase segregation approach (dotted curves) is observed.

Further, we investigate the nucleation of $In_xGa_{1-x}Sb$ NWs from quaternary In–Ga–Sb–Au alloy. As seen from the vertical section of the In–Ga–As–Au system at c_{tot} = 0.64 and c_{Sb} = 0.06 presented in Fig. 6, the compositional tuning of $In_xGa_{1-x}Sb$ throughout the entire compositional range is possible at $T < 430$ °C, which is the lowest temperature of the liquid single phase region. In comparison to As-based system, a relatively high Sb concentration c_{Sb} = 0.06 is needed to ensure positive difference of chemical potentials and, consequently, a positive supersaturation. Fig. 7 shows the liquid

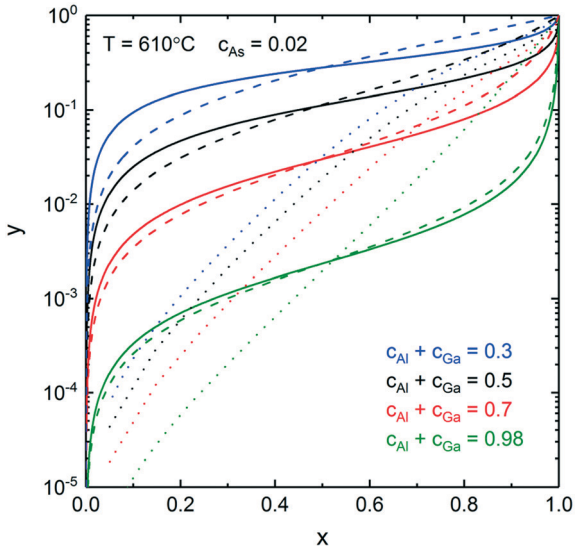

Fig. 5 Analytical calculations for the liquid–solid composition dependence of $Al_xGa_{1-x}As$ NWs for different c_{tot} at T = 610 °C and c_{As} = 0.02. The dotted curves are obtained using the phase segregation model. The dashed curves correspond to the model based on the one-parametric Langmuir expression with ε = 425 for c_{tot} = 0.98, ε = 32 for c_{tot} = 0.7, ε = 7.8 for c_{tot} = 0.5, and ε = 1.43 for c_{tot} = 0.3.

composition at c_{tot} = 0.64 and c_{Sb} = 0.06 plotted against the solid composition for different growth temperatures. The blue dashed curve at T = 450 °C indicates the absence of the solid phase and corresponds to the In molar fraction range within the 0.31–0.54 range on the GaSb–InSb vertical section of the In–Ga–Sb–Au phase diagram. When y decreases below 0.47, the solid phase occurs again (not shown in Fig. 7). The black dotted curve corresponds to the phase segregation model and is obtained using the Thermo-Calc software at T = 430 °C, c_{tot} = 0.64, and c_{Sb} = 0.06. It is seen that the analytical

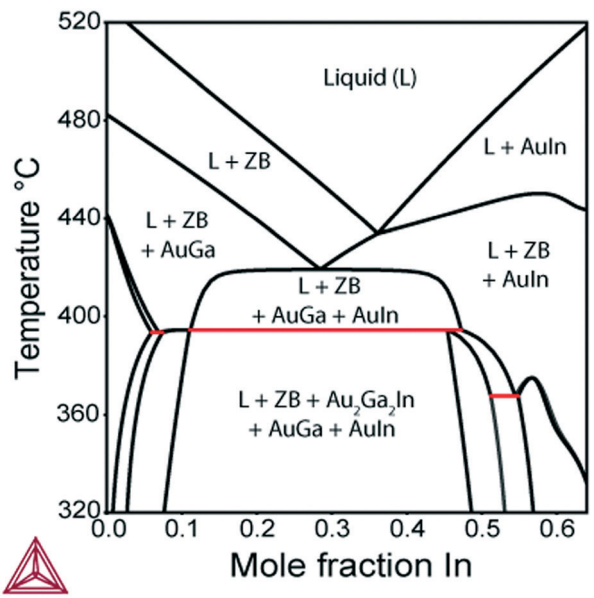

Fig. 6 Vertical section of the In–Ga–Sb–Au system at c_{tot} = 0.64 and c_{Sb} = 0.06.

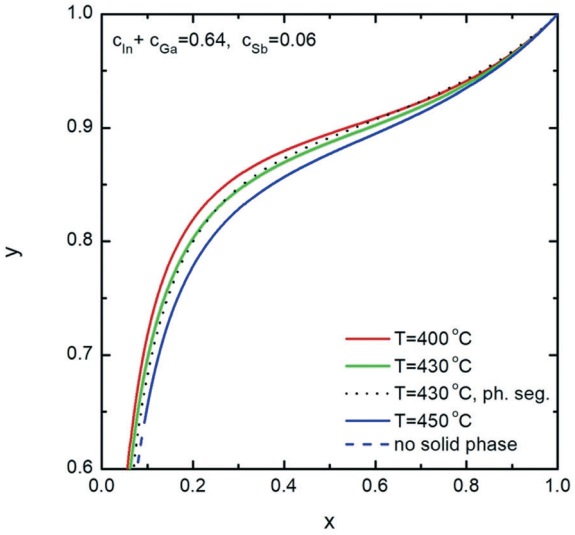

Fig. 7 Analytical calculations (solid curves) for the liquid–solid composition dependence of $In_xGa_{1-x}Sb$ NWs for different temperatures at c_{In} + c_{Ga} = 0.64 and c_{Sb} = 0.06. The dashed blue curve indicates the absence of solid $In_xGa_{1-x}Sb$ at these y-values. The dotted curve is obtained using the phase segregation model (T = 430 °C).

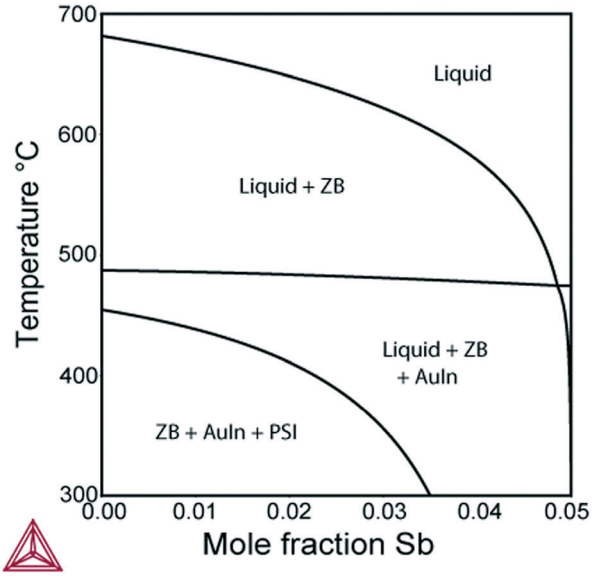

Fig. 9 Vertical section of the In–Sb–As–Au system at c_{In} = 0.45 and c_{tot} = 0.05.

model given by eqn (8) agrees well with the results of the phase segregation model. Fig. 8 shows the comparison of exact [given by eqn (8)] and approximate [eqn (11) and (12)] solutions for different total concentrations of group III elements and demonstrates a good agreement between them, especially for high x values. However, a significant divergence between exact and approximate solutions is observed for self-catalyzed growth.

Finally, we analyze nucleation of $InSb_xAs_{1-x}$ NWs from the In–Sb–As–Au melt. According to the phase diagram for the In–Sb–As–Au system presented in Fig. 9, the VLS growth of $InSb_xAs_{1-x}$ NWs is possible with any solid composition at T = 450 °C. The main feature of this system is the compositional-dependent pseudobinary interaction parameter. This results in a composition-dependent, asymmetric miscibility gap. Fig. 10 shows the liquid composition *versus* the $InSb_xAs_{1-x}$ solid composition for different temperatures in the cases of self-catalyzed (c_{tot} = 0.05 and c_{In} = 0.95) and gold-catalyzed growth at T = 450 °C (c_{tot} = 0.05 and c_{In} = 0.45). Defect-free, self-catalyzed NWs with an Sb fraction greater than x = 0.35 have been obtained at T = 520 °C, as reported in ref. 32. Such a relatively high value corresponds to $y \approx 0.975$. Clearly, it is

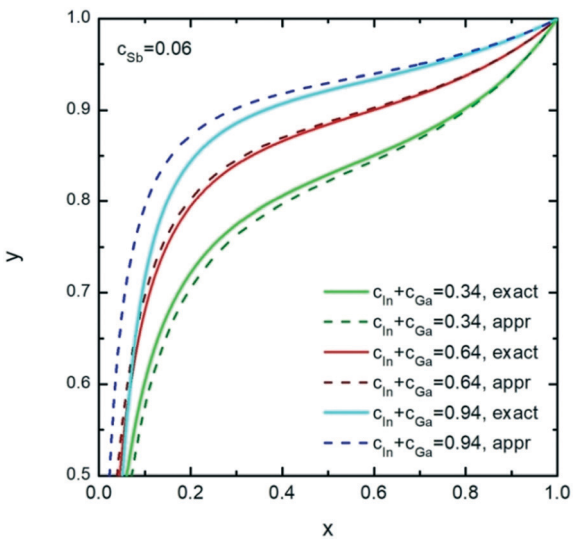

Fig. 8 Exact (solid curves) and approximate (dashed curves) solutions representing the liquid–solid composition dependences of solid $In_xGa_{1-x}Sb$ for different c_{tot} values at T = 430 °C and c_{As} = 0.06.

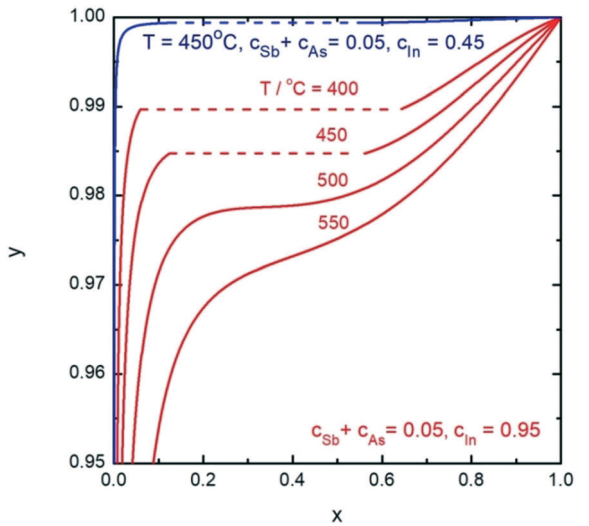

Fig. 10 Analytical calculations (solid curves) representing the liquid–solid composition dependences of solid $InSb_xAs_{1-x}$ NWs at c_{In} = 0.95 for different temperatures (red curves) and c_{In} = 0.45 at T = 450 °C (blue curve). The dashed part of the curves correspond to the miscibility gap.

more difficult to control the NW composition in the case of Au-catalyzed growth because of the much steeper slope of the $y(x)$ curve. Interestingly, in the case of $Al_xGa_{1-x}As$, the influence of the total concentration is reversed so that composition control would be easier in the Au-catalyzed case, as seen from comparing Fig. 5 and 10.

Conclusions

In summary, we have calculated the nucleation-limited compositions of ternary III–V NWs forming from quaternary alloys with gold. The calculations are based on realistic thermodynamic description and take into account ternary and composition-dependent binary interactions. We have analyzed the compositional diagrams for four highly relevant III–V materials systems. The results of this study show that the composition of ternary III–V NWs can be controlled over a wide range by tuning the composition of the catalyst droplet and temperature except for systems with high pseudobinary interaction parameters. For such systems ($In_xGa_{1-x}Sb$ and $In_xGa_{1-x}As$), formation of ternary NWs is thermodynamically forbidden in a wide range of solid compositions at relevant temperatures due to the miscibility gaps. In addition, we demonstrated that in many cases our analytical calculations are in good agreement with a purely thermodynamic phase segregation model.

Conflicts of interest

There are no conflicts of interest to declare.

Acknowledgements

This project has received funding from the European Union's Horizon 2020 research and innovation program under the Marie Skłodowska-Curie grant 722176 (project acronym INDEED). JJ and MG acknowledge financial support from NanoLund (the Center for Nanoscience at Lund University), the Swedish Research Council (VR) grant registration number 2015-04105, and the Knut and Alice Wallenberg Foundation (KAW). VGD thanks the Ministry of Education and Science of the Russian Federation for financial support under grant 14.587.21.0040 (project ID RFMEFI58717X0040).

References

1 A. I. Persson, M. W. Larsson, S. Stenström, B. J. Ohlsson, L. Samuelson and L. R. Wallenberg, *Nat. Mater.*, 2004, **3**, 677.
2 W. Lu and C. M. Lieber, *J. Phys. D: Appl. Phys.*, 2006, **39**, R387.
3 N. Wang, Y. Cai and R. Zhang, *Mater. Sci. Eng.*, 2008, **60**, 1.
4 B. Hua, J. Motohisa, S. Kobayashi, S. Hara and T. Fukui, *Nano Lett.*, 2009, **9**, 112.
5 G. Zheng, W. Lu, S. Jin and C. M. Lieber, *Adv. Mater.*, 2004, **16**, 1890.
6 A. Kandala, T. Betti and I. M. Fontcuberta, *Phys. Status Solidi*, 2009, **1**, 173.
7 H. Lee, M. Kim, I. Kim and H. Lee, *Adv. Mater.*, 2016, **28**, 4541.
8 D. R. Kim, C. H. Lee and X. Zheng, *Nano Lett.*, 2010, **10**, 1050–1054.
9 R. S. Wagner and W. C. Ellis, *Appl. Phys. Lett.*, 1964, **4**, 89.
10 C. Colombo, D. Spirkoska, M. Frimmer, G. Abstreiter and A. Fontcuberta i Morral, *Phys. Rev. B: Condens. Matter Mater. Phys.*, 2008, **77**, 155326.
11 F. Jabeen, V. Grillo, S. Rubini and F. Martelli, *Nanotechnology*, 2008, **19**, 275711.
12 V. G. Dubrovskii, T. Xu, A. Díaz Álvarez, S. R. Plissard, P. Caroff, F. Glas and B. Grandidier, *Nano Lett.*, 2015, **15**, 5580.
13 S. Plissard, K. A. Dick, G. Larrieu, S. Godey, A. Addad, X. Wallart and P. Caroff, *Nanotechnology*, 2010, **21**, 385602.
14 T. Grap, T. Rieger, C. Blömers, T. Schäpers, D. Grützmacher and M. I. Lepsa, *Nanotechnology*, 2013, **24**, 335601.
15 G. Priante, F. Glas, G. Patriarche, K. Pantzas, F. Oehler and J.-C. Harmand, *Nano Lett.*, 2016, **16**, 1917–1924.
16 C. S. Jung, H. S. Kim, G. B. Jung, K. J. Gong, Y. J. Cho, S. Y. Jang, C. H. Kim, C. W. Lee and J. Park, *J. Phys. Chem. C*, 2011, **115**, 7843–7850.
17 L. Li, D. Pan, Y. U. Xue, X. Wang, M. Lin, D. Su, Q. Zhang, X. Yu, H. So, D. Wei, B. Sun, P. Tan, A. Pan and J. Zhao, *Nano Lett.*, 2017, **17**, 622–630.
18 L. Namazi, S. G. Ghalamestani, S. Lehmann, R. R. Zamani and K. A. Dick, *Nanotechnology*, 2017, **28**, 165601.
19 S. G. Ghalamestani, M. Ek, B. Ganjipour, C. Thelander, J. Johansson, P. Caroff and K. A. Dick, *Nano Lett.*, 2012, **12**, 4914–4919.
20 V. G. Dubrovskii, A. A. Koryakin and N. V. Sibirev, *Mater. Des.*, 2017, **132**, 400–408.
21 V. G. Dubrovskii, *Cryst. Growth Des.*, 2015, **15**, 5738–5743.
22 J. Johansson and M. Ghasemi, *Phys. Rev. Mater.*, 2017, **1**, 040401(R).
23 F. Glas, *Cryst. Growth Des.*, 2017, **17**, 4785–4794.
24 J. Johansson and M. Ghasemi, *Cryst. Growth Des.*, 2017, **17**, 1630–1635.
25 G. Wilemski, *J. Phys. Chem.*, 1987, **91**, 2492–2498.
26 J. Grecenkov, V. G. Dubrovskii, M. Ghasemi and J. Johansson, *Cryst. Growth Des.*, 2016, **16**, 4526–4530.
27 J. Andersson, T. Helander, L. Höglund, P. Shi and B. Sundman, *Calphad*, 2002, **26**, 273–312.
28 J. C. Harmand, G. Patriarche, N. Péré-Laperne, M.-N. Mérat-Combes, L. Travers and F. Glas, *Appl. Phys. Lett.*, 2005, **87**, 203101.
29 F. Glas, J. C. Harmand and G. Patriarche, *Phys. Rev. Lett.*, 2007, **99**, 146101.
30 M. Heiss, B. Ketterer, E. Uccelli, J. R. Morante, J. Arbiol and A. Fontcuberta i Morral, *Nanotechnology*, 2011, **22**, 195601.
31 F. Jabeen, S. Rubini and F. Martelli, *Microelectron. J.*, 2009, **40**, 442–445.
32 H. Potts, M. Friedl, F. Amaduzzi, K. Tang, G. Tütüncüoglu, F. Matteini, E. A. Lladó, P. C. McIntyre and A. FontcubertaiMorral, *Nano Lett.*, 2016, **16**, 637–643.

Paper II

Journal of Crystal Growth 509 (2019) 118–123

Contents lists available at ScienceDirect

Journal of Crystal Growth

journal homepage: www.elsevier.com/locate/jcrysgro

Zinc blende and wurtzite crystal structure formation in gold catalyzed InGaAs nanowires

Jonas Johansson*, Egor D. Leshchenko

Solid State Physics and NanoLund, Lund University, Box 118, 221 00 Lund, Sweden

ARTICLE INFO

Communicated by J.M. Redwing

Keywords:
A1. Crystal structure
A1. Nanostructures
A1. Nucleation
B2. Semiconducting III-V materials
B2. Semiconducting ternary compounds

ABSTRACT

III-V semiconductor nanowires made of materials which have the zinc blende crystal structure in bulk are well known to exhibit either the zinc blende or the wurtzite crystal structure. Understanding and controlling which crystal structure that forms is of highest importance for nanowire applications in a variety of areas. In addition to this, composition control in ternary nanowires is another key technology area for successful nanowire applications. We derive a general model, based on two-component nucleation theory, which we use to explain the so far less understood experimental observations of zinc blende, wurtzite, and mixed crystal structure as a function of growth conditions and composition, x, in gold catalyzed $In_xGa_{1-x}As$ nanowires. An interesting theoretical finding is that the wurtzite and zinc blende phases have different compositions, even if they are nucleated from the same catalyst particle at the same conditions.

1. Introduction

Semiconductor nanowires (NWs) with controlled chemical composition [1], morphology [2], and size distribution [3] offer great promise in designing novel electronic [4], thermoelectric [5], and photovoltaic applications [6]. However, the incorporation of NW technology into semiconductor industry is still in its infancy and deeper understanding of NW formation processes is necessary for successful industrial and large scale implementations of NW fabrication.

It is well known that III-V NWs can grow in a crystal structure different from its bulk counterpart and that this can lead to formation of NWs with mixed crystal structure. For instance, GaAs having zinc blende (ZB) structure in bulk tends to form nanowires with ZB structure at low growth temperatures while wurtzite (WZ) is formed at high temperatures [7]. There is currently a lot of research about controlling the crystal structure of NWs by fine tuning the growth conditions and this is known as crystal phase control or crystal phase engineering. The breakthroughs in this area open new horizons allowing us to grow single-crystalline structures [8] or NWs with modulated crystal structures [9]. As the ZB and WZ structures have different band gaps, crystal phase superlattices can be fabricated for optoelectronic applications such as single-photon sources without using additional chemical elements and without composition modulation [10,11]. Switching between ZB and WZ can be achieved by varying the growth temperature and the precursor fluxes [12,13].

The vapor-liquid-solid (VLS) method [14], which is the most common method to fabricate semiconductor NWs has been developed to fulfill the requirements for control over the NW diameter and length, composition, crystal structure and growth direction. According to the VLS mechanism for III-V NWs, group III and group V materials supply the liquid droplets from the surrounding vapor forming a saturated, and when possible eutectic, alloy that catalyzes the NW growth when a certain supersaturation has been reached.

Previous attempts to crystal structure control are mainly devoted to binary III-V NWs. Crystal phase switching in GaAs NWs has recently been studied by Jacobsson et al [15] in terms of the NW-droplet interface morphology, the step-flow kinetics and the changes in droplet volume. Control of the crystal structure of Au-seeded III-V NWs of six materials (GaAs, InAs, GaP, InP, GaSb and InSb) over a variation of growth conditions has been demonstrated [7]. As an example of advanced crystal phase engineering, we note that InAs NW superlattices composed of 60 periods of ZB and WZ phase segments have been reported [9].

Crystal structure control in *ternary* NWs is, on the other hand, poorly studied. Among the various ternary material systems which are relevant for NW fabrication, the greatest attention has been paid to $In_xGa_{1-x}As$ NWs [1,8,13,16–24] due to its unique properties such as a tunable band gap over a wide range (0.35–1.42 eV), a very high electron mobility,

* Corresponding author.
E-mail address: jonas.johansson@ftf.lth.se (J. Johansson).
URL: http://www.nano.lu.se/jonas.johansson (J. Johansson).

https://doi.org/10.1016/j.jcrysgro.2019.01.002
Received 24 August 2018; Received in revised form 27 December 2018; Accepted 2 January 2019
Available online 03 January 2019

and a wide lattice constant range, which enables the growth of $In_xGa_{1-x}As$ NWs on many different substrates, and in particular these NWs are promising for Si integration [24]. However, growth investigations of Au-catalyzed $In_xGa_{1-x}As$ NWs are primarily aimed at composition control while the crystal structure of the fabricated NWs has been measured in addition to the main study. Experimentally it has been found that Au-catalyzed $In_xGa_{1-x}As$ NWs tend to form in ZB at low and high temperatures of 450 °C and 550 °C [8,16,17,20,21,23] whereas the NWs exhibit pure WZ or a WZ-dominant phase with some fraction of ZB in the middle of the temperature range (500 °C) [13,19]. In addition to temperature, the V/III flux ratio has drastic influence on the crystal structure of $In_xGa_{1-x}As$ NWs [13]. Moreover, structural analysis of catalyst-free $In_xGa_{1-x}As$ NWs has been reported [18,22].

The ability to fully control the NW crystal phase requires theoretical understanding and various explanations of the crystal structure formation in binary III-V NWs have been reported in the literature. A pioneering work, considering the occurrence of WZ in NWs of ZB semiconductors as a result of the energetic preference for the WZ nucleus formation over the ZB one at the triple phase line has been presented by Glas et al. [25] Moreover, it has been found that the probabilities of ZB and WZ phase formations depend on the liquid supersaturation and the material constants [26].

In this study, we report an approach to understanding the ZB and WZ crystal structure formation in ternary NWs growing from a quaternary Au-based liquid alloy. The developed model is based on thermodynamic considerations and two-component nucleation theory. We apply the model to $In_xGa_{1-x}As$ NWs and calculate the probabilities of ZB and WZ phase formation in this materials system and compare the obtained results with available experimental data. Special attention is paid to analysis of the main trends in crystal phase control and the impact of the liquid composition on the final crystal structure. The developed model may help in optimization of the growth conditions for growth of single-crystalline NWs or NWs with a modulated structure. Finally, an interesting effect in Au-catalyzed $In_xGa_{1-x}As$ NWs has been found, which could enable fabrication of NWs with ZB and WZ segments having different compositions even if the growth conditions are nominally constant.

2. Calculations

We consider the nucleation of a ternary nucleus of $A_xB_{1-x}D$ from a quaternary liquid drop consisting of A, B, D, U, where U is a solvent. The formation energy of such a nucleus [27] with crystal structure P (P is an abbreviation for polytype and denotes here ZB or WZ) can be expressed as

$$F_P(x, s) = -\Delta\mu_P(x, y)s + a_P(x)\sqrt{s}, \tag{1}$$

where $\Delta\mu_P$ is the chemical potential difference between the liquid particle and the solid nucleus with composition x and crystal structure P. The chemical potential difference is the driving force for nucleation and growth and is used as a measure of the supersaturation, that is the deviation from equilibrium. The parameter y denotes the fraction of A in the liquid, $y = c_A/c_{tot}$, where $c_{tot} = c_A + c_B$ and c_A and c_B are molar fractions. The chemical potential difference depends also on c_D, c_U, and temperature, T. The parameter s is the size of the nucleus (the total number of AD and BD pairs) and a_P is the effective surface energy of polytype P.

The chemical potentials are well described in Ref. [28] for the liquid and for the ZB phase. For the WZ phase we estimate the chemical potentials according to [26]

$$\mu_{AD}^{WZ} = \mu_{AD}^{ZB} + \psi_{AD} \tag{2a}$$

$$\mu_{BD}^{WZ} = \mu_{BD}^{ZB} + \psi_{BD}, \tag{2b}$$

where ψ_{AD} and ψ_{BD} are the differences in cohesive energy between the WZ and ZB phases for AD and BD, respectively. The composition and the size of the critical nucleus are given by the solutions to the equations

$$\frac{\partial F_P}{\partial x} = -\frac{\partial \Delta\mu_P}{\partial x}s + \frac{da_P}{dx}\sqrt{s} = 0 \tag{3}$$

and

$$\frac{\partial F_P}{\partial s} = -\Delta\mu_P + \frac{a_P}{2\sqrt{s}} = 0 \tag{4}$$

A simplifying remark [29] has recently been utilized [27,28] – that the surface energy of the critical nucleus is at a minimum due to surface segregation effects, so that $da_P/dx = 0$ at the critical composition. This leads to a simple expression for the composition of the critical nucleus as a function of the state of the particle

$$\frac{\partial \Delta\mu_P}{\partial x} = 0 \tag{5}$$

Since $\Delta\mu_{ZB} \neq \Delta\mu_{WZ}$, it follows that the solutions to Eq. (5), the critical compositions,

$$x_{ZB} \neq x_{WZ} \tag{6}$$

in general, which is our first main result.

In order to calculate the size of the critical nuclei, a model for the surface energy of these is needed. Based on the surface segregation argument [29], we simply set the surface energy of the critical nucleus equal to the surface energy of the one of the two pure materials with lowest surface energy for the respective polytype and denote this quantity a_P^*. Now we can express the sizes of the critical nuclei as

$$s_P = \frac{1}{4}\left[\frac{a_P^*}{\Delta\mu_P(x_P, y)}\right]^2 \tag{7}$$

and the nucleation barriers as

$$F_P^* = \frac{a_P^{*2}}{4\Delta\mu_P(x_P, y)} \tag{8}$$

In our approach to calculate the formation probabilities for the two different crystal structures, we estimate the nucleation rates as

$$J_{P,TPL} = A_{TPL}J_0 e^{-\frac{F_{P,TPL}^*}{RT}} \tag{9a}$$

$$J_{P,C} = A_C J_0 e^{-\frac{F_{P,C}^*}{RT}}, \tag{9b}$$

where we have considered both triple line (subscript TPL) and center (subscript C) nucleation [26], see schematic illustration in Fig. 1. One difference between these two cases is that the surface energies of the nuclei are different, leading to different nucleation barriers and different critical nucleus sizes. Also the areas on the NW growth interface where nucleation can occur are different. The factors A_{TPL} and A_C represent these areas for the respective case. If we model the nuclei as equilateral triangles with side length l_P (that is $l_{P,TPL}$ or $l_{P,C}$) and the NW growth interface as a regular hexagon with edge length R_{NW}, triple line nucleation occurs if one side of the nucleus is anchored at an edge of the growth interface. This can only happen if $l_{P,TPL} \leq R_{NW}$, in the other case triple line nucleation cannot happen. The considered geometry leads to $A_{TPL} = l_{P,TPL}(2R_{NW} - l_{P,TPL})3\sqrt{3}/2$ if $l_{P,TPL} \leq R_{NW}$ and $A_{TPL} = 0$ otherwise. Correspondingly, center nucleation can only occur if the entire nucleus has no edge length in common with the growth interface. This requires that the edge length of the nucleus, $l_{P,C} \leq \sqrt{3}R_{NW}$. In the other case, center nucleation is hindered. The area for center nucleation is equal to the area of the growth interface, $A_C = R_{NW}^2 3\sqrt{3}/2$ if $l_{P,C} \leq \sqrt{3}R_{NW}$ and $A_C = 0$ otherwise. The factor J_0 is a kinetic prefactor which depends on diffusivity, chemical potential differences, and temperature. In order to calculate NW growth rates, detailed modeling of J_0 is necessary. In our case, where we will only consider ratios of nucleation rates, it is a good approximation to consider the same J_0 for all cases, regardless of crystal structure and nucleation position. Finally,

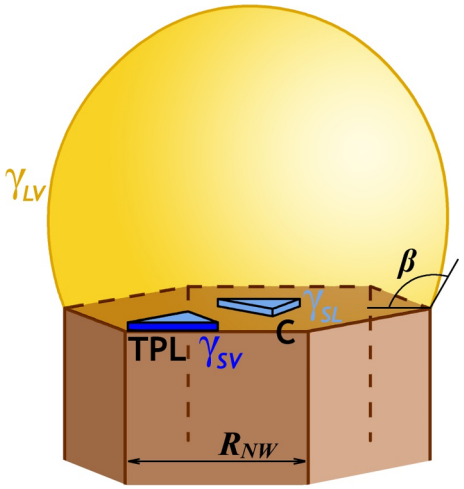

Fig. 1. Schematic illustration of the system. Two kinds of nucleation events are considered. One of these is nucleation along the triple line (TPL), with one edge of the nucleus along the triple line and the other two under the catalyst particle. The second one is center nucleation (C), where all three edges of the nucleus have contact with the catalyst particle.

for a triangular nucleus, l_P is given by

$$l_P = 2 \times 3^{-1/4}\sqrt{s_P \Omega_S / h}, \tag{10}$$

where Ω_S is the volume of a pair in the solid and h is the thickness of the nucleus.

The surface energy parameter of the critical nucleus can be expressed as $a_P^* = 2 \times 3^{3/4}\Gamma_P\sqrt{\Omega_S h}$, where Γ_P is the effective surface energy, given by [26,30]

$$\Gamma_P = \chi\gamma_{SL} + (1-\chi)\left(\gamma_{SV}\tau_P - \gamma_{LV}\frac{\Omega_L}{\Omega_S}\sin\beta\right), \tag{11}$$

where χ is the fraction of the edge length of the nucleus, which is not exposed to the vapor. That is, for triangular nuclei, $\chi = 2/3$ for triple line nucleation and $\chi = 1$ for center nucleation. The parameters, γ_{SL}, γ_{SV}, and γ_{LV}, account for the energies of the solid-liquid, solid-vapor, and liquid-vapor interfaces, respectively. Next we set $\tau_{ZB} = 1$, while $\tau_{WZ} < \tau_{ZB}$ to reflect that the surface energy is generally lower for the WZ than for the ZB crystal structure for the materials under consideration (III-V semiconductors). Of the remaining parameters, Ω_L is the volume of a pair in the liquid and β is the wetting angle.

Now we can express the probability for WZ crystal structure formation as a ratio of nucleation rates [26,31,32]

$$p_{WZ} = \frac{J_{WZ,TPL} + J_{WZ,C}}{J_{ZB,TPL} + J_{ZB,C} + J_{WZ,TPL} + J_{WZ,C}}. \tag{12}$$

The formation probability for ZB is then given by $p_{ZB} = 1 - p_{WZ}$.

3. Results and discussion

In this section, we analyze the WZ and ZB formation during growth of $In_xGa_{1-x}As$ NWs from a quaternary Au-based liquid alloy. As seen from Eqs. (8)–(12), the probability of crystal phase formation in NWs depends on several parameters including growth temperature, the droplet shape, the WZ/ZB surface energy ratio and the concentration of chemical elements in the liquid drop. Since the surface energies of InAs are lower than those of GaAs, we consider the surface energies of InAs for the critical nucleus. The surface energy of the liquid catalyst particle, γ_{LV}, is estimated as a linear interpolation of the surface energies of the constituting species, $\gamma_{LV} = yc_3\gamma_{In} + (1-y)c_3\gamma_{Ga} + (1-c_3)\gamma_{Au}$. Due to lack of surface energy data for As, we have replaced the surface energy of As with the one for Au [30]. Since the As concentration is very low, this should be a good approximation. The surface energies of the species in the liquid, as well as γ_{SV} and γ_{SL} are listed in Table 1. The chemical potentials are described in Ref. [28] and the cohesive energy differences used in the chemical potentials of the WZ phase, ψ_{InAs} and ψ_{GaAs}, are given in Table 1. Note that γ_{SV} and γ_{SL} are smaller for InAs than for GaAs. Thus, we use the values for InAs to calculate the effective surface energy of the critical nucleus. Here we point out that $In_xGa_{1-x}As$ has a miscibility gap at $T < 543$°C, meaning that some compositions are not thermodynamically stable at these temperatures [28]. Moreover, we perform all of our calculations for $R_{NW} = 100$ nm.

Table 1
Interface energies and cohesive energy differences used in the calculations. All the temperatures, T, have the unit K.

Property	Unit	Value	Reference
γ_{In}	J/m^2	$0.568 - 4\times10^{-5}(T-273) - 7.0\times10^{-8}(T-273)^2$	[36]
γ_{Ga}	J/m^2	$0.708 - 6.6\times10^{-5}(T-302.8)$	[37]
γ_{Au}	J/m^2	$1.15 - 1.4\times10^{-4}(T-1337)$	[38]
γ_{InAs}^{SL}	J/m^2	0.63	[30]
γ_{GaAs}^{SL}	J/m^2	0.73	[39]
γ_{InAs}^{SV}	J/m^2	1.19	[40]
γ_{GaAs}^{SV}	J/m^2	1.36	[41]
ψ_{InAs}	meV	17.6	[32]
ψ_{GaAs}	meV	23.1	[32]

We start by analyzing the temperature dependence of the probability of crystal phase formation and compare our numerical results to available experimental data. Fig. 2 shows the probability of WZ formation versus NW solid composition at $\beta = 130°$ and $\tau_{WZ} = 0.83$ according to ref. [26], $c_{As} = 0.018$ and $c_{Au} = 0.59$ (apart from the dashed curve where $c_{Au} = 0.713$) for different growth temperatures. It can be seen that the WZ phase prevails at $T = 500$°C over the entire range of the NW solid composition which is in agreement with the experimental investigations where pure WZ $In_{0.09}Ga_{0.91}As$ NWs [19] and NWs with a mixed phase of WZ and some ZB segments [13] were reported. The probability of WZ formation decreases when the temperature increases and the NWs tends to form in the ZB phase for $x > 0.2$ at $T = 520$°C, in agreement with Ref. [8]. However, WZ still prevails at low x values. A further increase in the growth temperature results in further narrowing

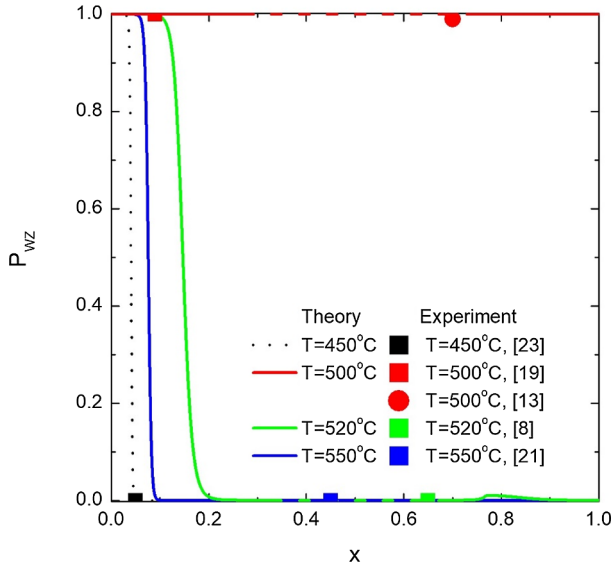

Fig. 2. The probability of WZ structure formation as a function of x in gold catalyzed $In_xGa_{1-x}As$ NWs at different growth temperatures. The solid and dotted curves are model calculations and the symbols represent experimental results from the literature. The dashed parts of the red, black and green curves indicate the miscibility gap.

of the WZ range, so ZB NWs with compositions of $x = 0.1$ or larger can be grown at $T = 550$°C.

For the formation of the WZ crystal structure it is necessary that the effective surface energy of WZ is significantly smaller than the corresponding one for the ZB structure. It is interesting to note that for this value of $\tau_{WZ} = 0.83$ and at conditions when all solid compositions can be reached (by varying y), pure GaAs ($x = 0$) always has the WZ structure. The composition, x, at which nucleation of the ZB phase becomes favorable depends on the supersaturation. The higher the supersaturation, the higher this cross-over composition and at sufficiently high supersaturation, also the pure InAs ($x = 1$) has the WZ structure. The supersaturation depends on the solubilities of In, Ga, and As in the Au-alloy particle. Since the solubility increases with increasing temperature [30], the supersaturation decreases with increasing temperature (for constant composition), which explains the temperature dependence of the cross-over composition. On a more specific level, the chemical potentials are functions of temperature and they influence the nucleation probabilities through the size and the composition of the critical nucleus.

At least three series of experiments of $In_xGa_{1-x}As$ NW growth at temperatures of 450–460 °C [13,17,23] indicated that NWs tends to form in the ZB phase at very low temperatures. To model this case, a higher Au concentration of $c_{Au} = 0.713$ was used, which might be explained by an increased difficulty of supersaturating the Au with Ga and As at these lower temperatures. As shown in Fig. 2 (dotted curve), this increase of c_{Au} reduces the WZ phase fraction and leads to the dominance of the ZB phase.

The dashed parts of the curves in Fig. 2 indicate the miscibility gap. In some cases, the NW growth is kinetically controlled and the experimental compositions are found in the miscibility gap. Even if these compositions are not thermodynamically stable, the nucleation probability as a function of composition is still expected to hold.

To simplify the analysis of the impact of growth temperature on the crystal phase, we limit ourselves to NWs whose droplet shape remains constant during growth. However, any unbalanced fluxes during growth can result in a droplet shape change, characterized by a variation of the contact angle. So, a group III element excess leads to swelling of the catalyst droplet. This effect has been reported for self-catalyzed growth of GaAs [2,33], where it is crucial to balance the group III and V fluxes. For Au catalyzed GaAs growth, larger wetting angles has been observed at low V/III-ratio both during MBE [34] and MOVPE [35]. The probability of WZ formation as a function of the NW composition for several different wetting angles is presented in Fig. 3. The wetting angles range from $\beta = 90°$ to $\beta = 130°$, corresponding to most experimental observations and the two extreme values correspond to stable nanowire growth [2]. The other parameters are $\tau_{WZ} = 0.83$, $c_{As} = 0.018$, $c_{Au} = 0.59$, and $T = 520$°C. As shown in Fig. 3, the $p_{WZ}(x)$ for the two stable contact angles is different around the miscibility gap and at high x values. At compositions $0.7 < x < 1$ the ZB crystal structure is the dominant phase for $\beta = 130°$, whereas it is WZ for $\beta = 90°$. This means that the change of the droplet shape during growth of NWs with high enough x values may result in an unwanted, mixed crystal structure. A similar dependence of NW crystal structure on the contact angle has been experimentally observed during growth of GaAs NWs [15]. Thus, for the synthesis of single phase NWs, the growth conditions should as much as possible prohibit any droplet shape fluctuations.

The non-monotonic composition dependence of $p_{WZ}(x)$, which is obtained at some conditions (see for instance the $\beta = 90°$ curve in Fig. 3) originates from the nucleation rates of WZ and ZB at the triple phase line or in the center of the liquid-solid interface. In Fig. 4, these nucleation rates are shown as a function of y for the same parameters as the previous figure. The reason for showing them as a function of y is that y uniquely describes the state of the system, whereas the solid composition depends on which crystal phase that is considered [see Eq. (6)]. At low y values and at these parameters, WZ phase nucleation at the triple phase line dominates which changes to ZB phase nucleation at

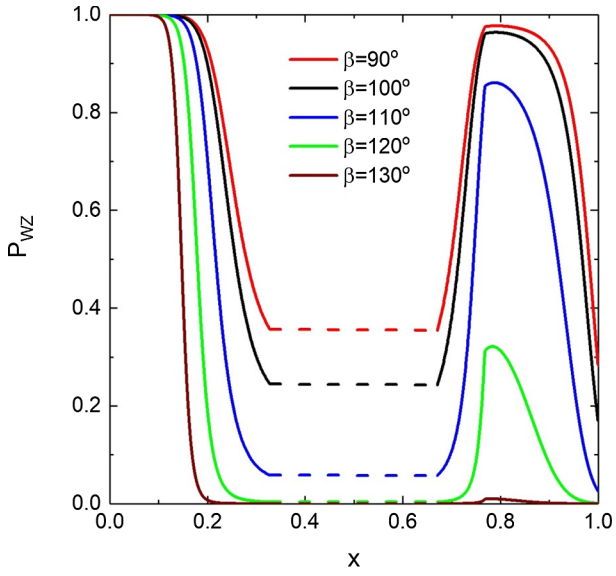

Fig. 3. The probability of WZ structure formation as a function of x in gold catalyzed $In_xGa_{1-x}As$ NWs calculated at different wetting angles. As in Fig. 2, the dashed parts of the curves indicate the miscibility gap.

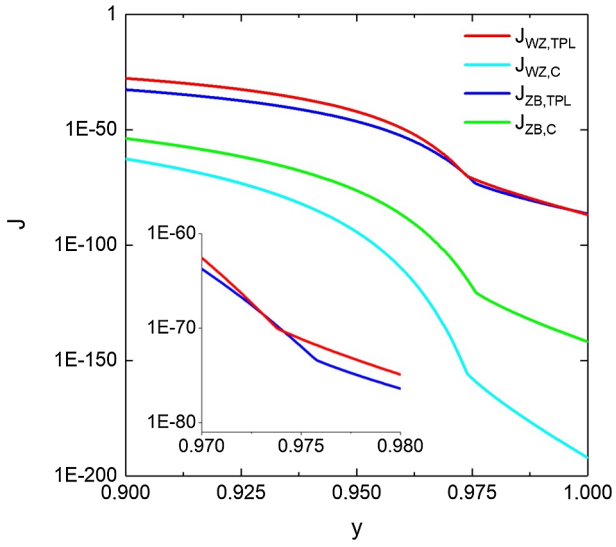

Fig. 4. The nucleation rates in arbitrary unit for triple line, TPL, and center, C, nucleation of WZ and ZB structure as a function of the composition of the liquid catalyst, y. The inset is a zoom in on the WZ and ZB TPL curves, indicating their crossings.

y= 0.973 to 0.974 (see inset) and back to WZ at higher y values to finally change to ZB at the highest values of y. At $y \approx 0.974$, the miscibility gap compositions are reached in the solid, which leads to a discontinuity of the chemical potential difference due to a sudden jump in x. This, in turn, causes kinks in the nucleation rates. It should be noted that while nucleation of ZB in the center of the liquid-solid interface and nucleation of ZB and WZ at the triple phase line can be obtained under different growth conditions, nucleation of WZ in the center of the liquid-solid interface is always unfavorable and suppressed. Specifically, if the temperature is decreased to $T = 500$°C and the other parameters are the same, then TPL nucleation of WZ dominates for all values of y (see the red curve in Fig. 2).

Fig. 5 shows the liquid droplet composition, y, versus the $In_xGa_{1-x}As$ solid composition at $T = 520$°C, $c_{As} = 0.018$, $\beta = 90°$ and $c_{Au} = 0.59$ in the case of WZ and ZB phase nucleation. For the same y-values, we see that the solid compositions of WZ and ZB NWs tends to the same values

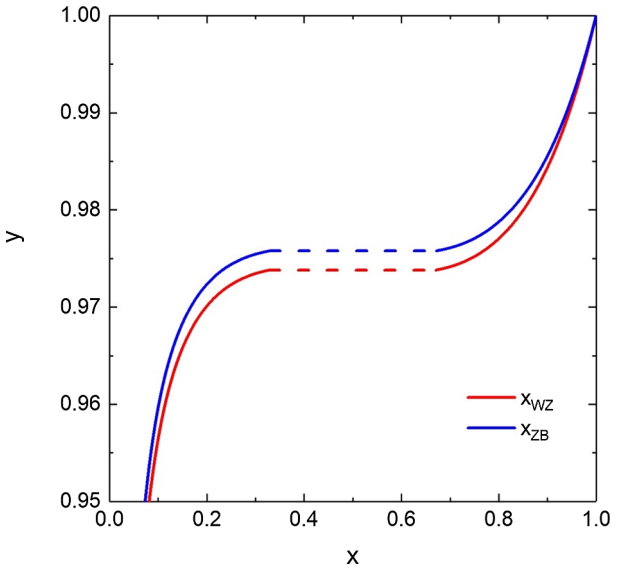

Fig. 5. The composition of the liquid catalyst, y, as a function of the composition, x, of the solid $In_xGa_{1-x}As$ NWs for both WZ and ZB phase nucleation. The dashed parts of the curves indicate the miscibility gap.

in the limit of low and high x, while they split up in the middle x region. Due to the flat shape of the curves, this splitting up leads to the possibility of two significantly different solid compositions at one y-value. This means that it is theoretically possible to synthesize superlattice structure consisting of ZB segments with low x and WZ ones with high x value without any change of growth conditions. Whether this is practically feasible or not, depends on the nucleation probabilities in the narrow interval of y-values between the flat parts of the composition curves.

The liquid composition $y = 0.974$ lies in this interval and since the dominating nucleation rates cross at this composition (see inset in Fig. 4), $p_{WZ} \approx 0.5$. In Fig. 5 we see that the compositions of WZ and ZB are $x_{WZ} \approx 0.74$ and $x_{ZB} \approx 0.24$ at this value of y. Our nucleation probability calculations show that any fluctuation in the liquid composition leading to a small increase in y results in almost pure WZ and a small decrease in y can lead to a mixed crystal structure dominated by ZB. This effect could also occur at different growth conditions and with a detailed modeling of the exponential prefactors in the nucleation rates. The requirement is that the dominating nucleation rates for WZ and ZB cross at y-values between the miscibility gaps of the solid phases, similar to the crossing at $y = 0.974$ in the inset in Fig. 4.

4. Conclusions

Using two-component nucleation theory, we have proposed a model for the composition dependence of the WZ-ZB polytypism in ternary nanowires growing by the VLS mechanism. The model is general and we apply it to gold-catalyzed growth of $In_xGa_{1-x}As$ nanowires. Using the model we are able to explain experimentally observed features of WZ and ZB crystal structure formation in this widely investigated material.

Specifically we find that at conditions, where all solid compositions can be reached by varying the composition of the catalyst particle, WZ is always favorable at low x. At high x, on the other hand, either WZ or ZB can be favorable, depending on the supersaturation. At high supersaturation, WZ forms, in agreement with previous investigations for binary materials.

An interesting theoretical result is that the WZ and ZB phases have different compositions, even if they are nucleated from identical conditions of the catalyst particle. This opens up for a possibility to fabricate WZ-ZB superlattices with different compositions in the different crystal phases. Whether this is feasible or not depends on the nucleation probabilities. Our calculations indicate that this can indeed be feasible at growth temperatures where a miscibility gap exists, provided that the supersaturation is high enough.

Acknowledgements

This project has received funding from the European Union's Horizon 2020 research and innovation program under the Marie Skłodowska-Curie grant 722176 (project acronym INDEED). JJ acknowledges financial support from the Swedish Research Council (VR) grant registration number 2015-04105.

References

[1] C.S. Jung, H.S. Kim, G.B. Jung, K.J. Gong, Y.J. Cho, S.Y. Jang, C.H. Kim, C.W. Lee, J. Park, Composition and phase tuned InGaAs alloy nanowires, J. Phys. Chem. C 115 (2011) 7843–7850.
[2] W. Kim, V.G. Dubrovskii, J. Vukajlovic-Plestina, G. Tutuncuoglu, L. Francaviglia, L. Guniat, H. Potts, M. Friedl, J.B. Leran, A.F.I. Morral, Bistability of contact angle and its role in achieving quantum-thin self-assisted GaAs nanowires, Nano Lett. 18 (2018) 49–57.
[3] V.G. Dubrovskii, T. Xu, A.D. Alvarez, S.R. Plissard, P. Caroff, F. Glas, B. Grandidier, Self-equilibration of the diameter of Ga-catalyzed GaAs nanowires, Nano Lett. 15 (2015) 5580–5584.
[4] O.P. Kilpi, J. Svensson, J. Wu, A.R. Persson, R. Wallenberg, E. Lind, L.E. Wernersson, Vertical InAs/InGaAs heterostructure metal-oxide-semiconductor field-effect transistors on Si, Nano Lett. 17 (2017) 6006–6010.
[5] J. Gooth, J.G. Gluschke, R. Zierold, M. Leijnse, H. Linke, K. Nielsch, Thermoelectric performance of classical topological insulator nanowires, Semicond. Sci. Tech. 30 (2015) 015015.
[6] M.T. Borgstrom, M.H. Magnusson, F. Dimroth, G. Siefer, O. Hohn, H. Riel, H. Schmid, S. Wirths, M. Bjork, I. Aberg, W. Peijnenburg, M. Vijver, M. Tchernycheva, V. Piazza, L. Samuelson, Towards nanowire tandem junction solar cells on silicon, IEEE J. Photovolt. 8 (2018) 733–740.
[7] K.A. Dick, P. Caroff, J. Bolinsson, M.E. Messing, J. Johansson, K. Deppert, L.R. Wallenberg, L. Samuelson, Control of III-V nanowire crystal structure by growth parameter tuning, Semicond. Sci. Technol. 25 (2010) 024009.
[8] H. Tan, C. Fan, L. Ma, X.H. Zhang, P. Fan, Y.K. Yang, W. Hu, H. Zhou, X.J. Zhuang, X.L. Zhu, A.L. Pan, Single-crystalline InGaAs nanowires for room-temperature high-performance near-infrared photodetectors, Nano-Micro Lett. 8 (2016) 29–35.
[9] K.A. Dick, C. Thelander, L. Samuelson, P. Caroff, Crystal phase engineering in single InAs nanowires, Nano Lett. 10 (2010) 3494–3499.
[10] D. Spirkoska, J. Arbiol, A. Gustafsson, S. Conesa-Boj, F. Glas, I. Zardo, M. Heigoldt, M.H. Gass, A.L. Bleloch, S. Estrade, M. Kaniber, J. Rossler, F. Peiro, J.R. Morante, G. Abstreiter, L. Samuelson, A.F.I. Morral, Structural and optical properties of high quality zinc-blende/wurtzite GaAs nanowire heterostructures, Phys. Rev. B 80 (2009) 24325.
[11] N. Akopian, G. Patriarche, L. Liu, J.C. Harmand, V. Zwiller, Crystal phase quantum dots, Nano Lett. 10 (2010) 1198–1201.
[12] P. Caroff, K.A. Dick, J. Johansson, M.E. Messing, K. Deppert, L. Samuelson, Controlled polytypic and twin-plane superlattices in III-V nanowires, Nat. Nanotechnol. 4 (2009) 50–55.
[13] A.S. Ameruddin, H.A. Fonseka, P. Caroff, J. Wong-Leung, R.L.M.O.H. Veld, J.L. Boland, M.B. Johnston, H.H. Tan, C. Jagadish, InxGa1-xAs nanowires with uniform composition, pure wurtzite crystal phase and taper-free morphology, Nanotechnology 26 (2015) 205604.
[14] R.S. Wagner, W.C. Ellis, Vapor-liquid-solid mechanism of single crystal growth, Appl. Phys. Lett. 4 (1964) 89.
[15] D. Jacobsson, F. Panciera, J. Tersoff, M.C. Reuter, S. Lehmann, S. Hofmann, K.A. Dick, F.M. Ross, Interface dynamics and crystal phase switching in GaAs nanowires, Nature 531 (2016) 317–326.
[16] Y. Kim, H.J. Joyce, O. Gao, H.H. Tan, C. Jagadish, M. Paladugu, J. Zou, A.A. Suvorova, Influence of nanowire density on the shape and optical properties of ternary InGaAs nanowires, Nano Lett. 6 (2006) 599–604.
[17] K. Tateno, G.Q. Zhang, H. Nakano, Growth of GaInAs/AlInAs heterostructure nanowires for long-wavelength photon emission, Nano Lett. 8 (2008) 3645–3650.
[18] J.C. Shin, K.H. Kim, K.J. Yu, H.F. Hu, L.J. Yin, C.Z. Ning, J.A. Rogers, J.M. Zuo, X.L. Li, InxGa1-xAs nanowires on silicon: one-dimensional heterogeneous epitaxy, Bandgap Engineering, and Photovoltaics, Nano Lett. 11 (2011) 4831–4838.
[19] F. Jabeen, V. Grillo, F. Martelli, S. Rubini, InGaAs/GaAs core-shell nanowires grown by molecular beam epitaxy, IEEE J. Sel. Top. Quant. 17 (2011) 794–800.
[20] J.J. Hou, N. Han, F.Y. Wang, F. Xiu, S.P. Yip, A.T. Hui, T.F. Hung, J.C. Ho, Synthesis and characterizations of ternary InGaAs nanowires by a two-step growth method for high-performance electronic devices, Acs Nano 6 (2012) 3624–3630.
[21] J.J. Hou, F.Y. Wang, N. Han, F. Xiu, S.P. Yip, M. Fang, H. Lin, T.F. Hung, J.C. Ho, Stoichiometric effect on electrical, optical, and structural properties of composition-tunable InxGa1-xAs nanowires, Acs Nano 6 (2012) 9320–9325.
[22] S. Morkötter, S. Funk, M. Liang, M. Doblinger, S. Hertenberger, J. Treu, D. Rudolph, A. Yadav, J. Becker, M. Bichler, G. Scarpa, P. Lugli, I. Zardo, J.J. Finley, G. Abstreiter, G. Koblmuller, Role of microstructure on optical properties in high-uniformity In1-xGaxAs nanowire arrays: evidence of a wider wurtzite band gap,

Phys. Rev. B 87 (2013) 205303.
[23] Y.N. Guo, H.Y. Xu, G.J. Auchterlonie, T. Burgess, H.J. Joyce, Q. Gao, H.H. Tan, C. Jagadish, H.B. Shu, X.S. Chen, W. Lu, Y. Kim, J. Zou, Phase separation induced by Au catalysts in ternary InGaAs nanowires, Nano Lett. 13 (2013) 643–650.
[24] G. Koblmuller, G. Abstreiter, Growth and properties of InGaAs nanowires on silicon, Phys. Status Solidi RRL 8 (2014) 11–30.
[25] F. Glas, J.C. Harmand, G. Patriarch, Why does wurtzite form in nanowires of III-V zinc blende semiconductors? Phys. Rev. Lett. 99 (2007) 146101.
[26] V.G. Dubrovskii, N.V. Sibirev, J.C. Harmand, F. Glas, Growth kinetics and crystal structure of semiconductor nanowires, Phys. Rev. B 78 (2008) 235301.
[27] V.G. Dubrovskii, A.A. Koryakin, N.V. Sibirev, Understanding the composition of ternary III-V nanowires and axial nanowire heterostructures in nucleation-limited regime, Mater. Design 132 (2017) 400–408.
[28] E.D. Leshchenko, M. Ghasemi, V.G. Dubrovskii, J. Johansson, Nucleation-limited composition of ternary III-V nanowires forming from quaternary gold based liquid alloys, CrystEngComm 20 (2018) 1649–1655.
[29] G. Wilemski, Revised classical binary nucleation theory for aqueous alcohol and acetone vapors, J. Phys. Chem. 91 (1987) 2492–2498.
[30] J. Johansson, M. Ghasemi, Composition of gold alloy seeded InGaAs nanowires in the nucleation limited regime, Cryst. Growth Des. 17 (2017) 1630–1635.
[31] J. Johansson, L.S. Karlsson, K.A. Dick, J. Bolinsson, B.A. Wacaser, K. Deppert, L. Samuelson, Effects of supersaturation on the crystal structure of gold seeded III-V nanowires, Cryst. Growth Des. 9 (2009) 766–773.
[32] J. Johansson, Z. Zanolli, K.A. Dick, Polytype attainability in III-V semiconductor nanowires, Cryst. Growth Des. 16 (2016) 371–379.
[33] G. Priante, S. Ambrosini, V.G. Dubrovskii, A. Franciosi, S. Rubini, Stopping and resuming at will the growth of GaAs nanowires, Cryst. Growth Des. 13 (2013) 3976–3984.
[34] D.L. Dheeraj, A.M. Munshi, M. Scheffler, A.T.J. van Helvoort, H. Weman, B.O. Fimland, Controlling crystal phases in GaAs nanowires grown by Au-assisted molecular beam epitaxy, Nanotechnology 24 (2013) 015601.
[35] S. Lehmann, D. Jacobsson, K.A. Dick, Crystal phase control in GaAs nanowires: opposing trends in the Ga- and As-limited growth regimes, Nanotechnology 26 (2015) 301001.
[36] D.W.G. White, The surface tensions of indium and cadmium, Metall. Trans. 3 (1972) 1933–1936.
[37] S.C. Hardy, The surface-tension of liquid gallium, J. Cryst. Growth 71 (1985) 602–606.
[38] I. Egry, G. Lohoefer, G. Jacobs, Surface-tension of liquid-metals - results from measurements on ground and in-space, Phys. Rev. Lett. 75 (1995) 4043–4046.
[39] S. Sakong, Y.A. Du, P. Kratzer, Atomistic modeling of the Au droplet-GaAs interface for size-selective nanowire growth, Phys. Rev. B 88 (2013) 155309.
[40] N. Moll, M. Scheffler, E. Pehlke, Influence of surface stress on the equilibrium shape of strained quantum dots, Phys. Rev. B 58 (1998) 4566–4571.
[41] N. Moll, A. Kley, E. Pehlke, M. Scheffler, GaAs equilibrium crystal shape from first principles, Phys. Rev. B 54 (1996) 8844–8855.